bioRxiv preprint doi: https://doi.org/10.1101/2020.04.27.063628; this version posted April 28, 2020. The copyright holder for this preprint (which was not certified by peer review) is the author/funder, who has granted bioRxiv a license to display the preprint in perpetuity. It is made available under aCC-BY-NC-ND 4.0 International license.

Toxoplasma ferlin1 is a versatile and dynamic mediator of microneme trafficking and secretion

Daniel N.A. Tagoe[1], Allison A. Drozda[1], Isabelle Coppens[2], Bradley I. Coleman[1†], Marc-Jan Gubbels[1§]

[1]Biology Department of Biology, Boston College, Chestnut Hill, MA 02467, USA

[2]Department of Molecular Microbiology and Immunology, Johns Hopkins University Bloomberg School of Public Health, Baltimore, Maryland, USA

[§]Correspondence to Marc-Jan Gubbels, gubbelsj@bc.edu

[†]Present address: Bradley. I Coleman, Harvard Medical School, Boston, Massachusetts, USA

Running title: *Toxoplasma* ferlin 1 acts on micronemes

bioRxiv preprint doi: https://doi.org/10.1101/2020.04.27.063628; this version posted April 28, 2020. The copyright holder for this preprint (which was not certified by peer review) is the author/funder, who has granted bioRxiv a license to display the preprint in perpetuity. It is made available under aCC-BY-NC-ND 4.0 International license.

Abstract

Calcium-dependent exocytosis of the microneme organelles that facilitate host cell invasion is critical for obligate intracellular apicomplexan parasites such as *Toxoplasma gondii*. Ferlins represent a protein family with roles in exocytosis containing multiple Ca^{2+}-sensing C2 domains. Here we defined the role of *T. gondii*'s ferlin 1 (FER1) in microneme biology. FER1 localized dynamically to several compartments of the parasite's secretory pathway as well as to an apical spot near the site of microneme secretion. FER1 function was dissected by overexpression of a variety of N-terminally tagged alleles causing dominant negative phenotypes. This demonstrated FER1 traffics microneme organelles at several discrete steps of their natural trajectories: 1. from ELC to the subpellicular microtubules; 2. along the subpellicular microtubules to the apical end; 3. into the conoid; 4. and inferred from observed retrograde transport from the subpellicular microtubules, recycling of micronemes from mother to daughter parasites. Furthermore, full-length FER1 overexpression results in a squirt of microneme release sufficient for host cell egress. This indicates FER1 facilitates fusion of the most apical, radially organized micronemes with the plasma membrane. Moreover, FER1 acts differentially on the Rab5A/C-dependent and -independent microneme sub-populations. Finally, apical FER1 overlaps with the presence of VP1, a pyrophosphatase proton pump. Integrating all new insights, we propose a model of microneme exocytosis wherein the radial micronemes constitute a readily releasable vesicle pool primed by acidification.

Keywords: exocytosis/calcium/ferlin/microneme/trafficking/*Toxoplasma*

bioRxiv preprint doi: https://doi.org/10.1101/2020.04.27.063628; this version posted April 28, 2020. The copyright holder for this preprint (which was not certified by peer review) is the author/funder, who has granted bioRxiv a license to display the preprint in perpetuity. It is made available under aCC-BY-NC-ND 4.0 International license.

Introduction

In humans, the apicomplexan parasite *Toxoplasma gondii* causes birth defects, vision loss, myocarditis and encephalitis. Lytic replication cycles unfolding through repetitive rounds of host cell invasion, intracellular replication and host cell egress are central to the pathogenesis of toxoplasmosis [1]. The micronemes in apicomplexan parasites are pivotal for successful host cell invasion as they contain adhesion molecules facilitating gliding motility and host cell association [2, 3]. In addition, the *Toxoplasma gondii* micronemes encode a pore-forming protein, PLP1, that permeabilizes both the parasitophorous vacuole and host plasma membrane, which is required for efficient host cell egress [4, 5]. The parasite's signal transduction pathways controlling the correct timing of micronemes secretion comprises cGMP, Ca^{2+} and phosphatidic acid (PA) [6], accompanied by a crucial cAMP-mediated switch between the intracellular and extracellular states [7].

The micronemes are localized along the apical cortex in association with the subpellicular microtubules emanating from the apical end [8, 9]. Upon activation of secretion, micronemes move into the conoid, a tubulin basket at the very apical tip of the parasites, to fuse with the plasma membrane. Following secretion, microneme protein complexes are embedded in the plasma membrane with the extracellular domains serving as adhesion domains and the cytoplasmic tail engaging with actin filaments that are transported in an apical to basal direction by a myosin motor anchored in the membrane skeleton [10]. The working model is that sustainable microneme secretion is dosed to support prolonged periods of gliding motility to cross biological barriers in between host cells. Dosing is most likely achieved by gradually trafficking micronemes aligned on the subpellicular microtubules toward the conoid to avoid bulk micronemal content release. In addition, a set of radial micronemes organized and anchored just below the conoid is believed to be a readily-releasable pool of micronemes [11-13].

Biogenesis of the micronemes and trafficking of microneme proteins progresses through the secretory pathway comprising sequential passage through the endoplasmic reticulum (ER), Golgi apparatus, trans-Golgi Network (TGN) and an endosome like compartment (ELC) [14-16]. Many secretory proteins undergo proteolytic processing to remove their pro-peptide mediated by the plant like vacuole (VAC or PLV), an acidic compartment [17-20]. Protein sorting to both microneme and rhoptry organelles requires sortilin (SORTLR) [21] whereas the HOPS/CORVET complex and Rab7 are involved in PLV/VAC routing [22]. Moreover, adaptor

bioRxiv preprint doi: https://doi.org/10.1101/2020.04.27.063628; this version posted April 28, 2020. The copyright holder for this preprint (which was not certified by peer review) is the author/funder, who has granted bioRxiv a license to display the preprint in perpetuity. It is made available under aCC-BY-NC-ND 4.0 International license.

complex AP1 is involved in microneme and rhoptry protein trafficking, but has a more general function across other vesicular trafficking events [23]. Although some rhoptry specific targeting signals have been identified [24, 25], specific sorting signals for microneme proteins are still elusive. Specific Rab GTPases have been associated with some aspects of microneme protein trafficking, and actually differentiate two sub-populations of micronemes with a different protein content: one of which is Rab5A/C-dependent, and one that is Rab5A/C-independent [9]. Consequently, specific microneme proteins end up in different, non-overlapping microneme sub-populations. The exocytosis event at the very apical tip has been associated with Centrin2 [26] and double C2 (TgDOC2) [27], both of which are Ca^{2+}-binding proteins. Furthermore, the association of an acylated pleckstrin homology (PH) domain-containing protein (APH) on the surface of the micronemes with PA deposited in the plasma membrane is essential for exocytosis and aid in timing membrane fusion [28]. In addition, Rab11a is present at the very apical end of the parasite and is required for efficient microneme exocytosis, though Rab11a's function is not exclusively acting on the micronemes and is much more varied [29]. The proposed membrane fusion model comprises v- and t-SNAREs on the microneme limiting membrane and the plasma membrane, respectively, where TgDOC2, mediates the Ca^{2+} regulation, which together with Rab11a and the APH-PA interaction pull the membranes together toward their fusion [6, 30]. However, the identity of such SNAREs is still elusive. Finally, sustained microneme secretion in extracellular parasites is balanced with active endocytosis [31], whereas during cell division micronemes of the mother are re-directed into the newly forming daughters [32].

In all the well-studied Ca^{2+} triggered exocytosis systems, proteins containing double C2, (DOC2) domains execute the Ca^{2+}-mediated vesicle fusion [33]. C2 domains are approximately 150 amino acids in length and composed of eight beta strands that insert into a membrane or associate with other proteins, some of which are conditional upon the presence of Ca^{2+} [33, 34]. Binding of Ca^{2+} and/or phospholipids is facilitated by specifically positioned residues in three loops extending from the C2 domain. Aspartate residues, and to some extent glutamate, create a negatively charged binding pocket that permits Ca^{2+} binding [35-37]. The binding of Ca^{2+} leads to conformational changes facilitating insertion into a membrane or lipid binding via a calcium bridge [38, 39]. Alternatively, asparagine in these positions, eliminates the negative charge, and promotes phospholipid binding independent of Ca^{2+} [36, 37]. Typically, at least one membrane associated and one soluble DOC2 protein are needed to facilitate Ca^{2+}-dependent fusion. We

bioRxiv preprint doi: https://doi.org/10.1101/2020.04.27.063628; this version posted April 28, 2020. The copyright holder for this preprint (which was not certified by peer review) is the author/funder, who has granted bioRxiv a license to display the preprint in perpetuity. It is made available under aCC-BY-NC-ND 4.0 International license.

have previously identified a soluble TgDOC2 protein essential for *Toxoplasma* microneme secretion [27]. The ferlins make up a unique branch of the DOC2 domain protein family because they are relatively large (200-240 kDa) and contain five to seven C2 domains rather than two, which are typically organized in C2 pairs to form 2-3 DOC2 domains. The extended C2 repertoire in ferlins has broadened their functional spectrum beyond membrane fusion to vesicle trafficking and membrane repair [40]. Mammalian ferlins come in two flavors differentiated by their sub-cellular localization at either the plasma membrane or on intracellular compartments, which relates to their function in either late endosomal transit versus trans-Golgi recycling [41]. Mammalian otoferlin, essential for neurotransmitter release from the inner hair cells (IHC) in the auditory system, has been most widely studied. Otoferlin functions as both a scaffolding protein in the secretory pathway as well as in the actual membrane fusion during exocytosis [42-45].

The Apicomplexa encode two conserved ferlin proteins, FER1 and FER2, but some parasites, including *T. gondii*, encode a degenerate third ferlin [46]. FER1 in *Plasmodium berghei,* named ferlin-like protein (PbFLP), was recently reported to be essential for male gametocyte egress [47], whereas we showed that *Toxoplasma* FER2 is required for rhoptry secretion [46]. Here we examined the function of FER1 in microneme protein trafficking, microneme dynamics and secretion in the *Toxoplasma gondii* lytic cycle.

Results

1. *Toxoplasma* FER1 localizes to the secretory pathway and a discrete apical region

In the genome wide fitness screen for the *Toxoplasma* lytic cycle FER1 (TGGT1_309420) has a severe fitness score of -4.77, strongly indicating that this protein is essential [48]. The critical role of FER1 in the lytic cycle was underscored in our unsuccessful efforts to generate either an endogenously tagged allele at either the N- or C-terminus to determine its sub-cellular localization. Since FER1 is a tail-anchored transmembrane (TM) domain containing protein ([49], Fig 1A), we reasoned that we could resolve its subcellular localization through fusion of the terminal transmembrane (TM) domain including the extreme C-terminal cytoplasmic tail to a YFP reporter. Transient transfection of parasites with an α-tubulin promoter driven fusion construct encoding the C-terminal 31 aa (comprising the 10 aa before the extreme C-terminal and the 21 aa long TM domain) resulted in YFP signal in an extremely apical, conoid-associated

bioRxiv preprint doi: https://doi.org/10.1101/2020.04.27.063628; this version posted April 28, 2020. The copyright holder for this preprint (which was not certified by peer review) is the author/funder, who has granted bioRxiv a license to display the preprint in perpetuity. It is made available under aCC-BY-NC-ND 4.0 International license.

region as well as in the perinuclear region (Fig 1B). This indicates that FER1 localizes to the endoplasmic reticulum surrounding the nucleus as well as to the very apical tip of the parasite from where microneme and rhoptry organelle exocytosis takes place. To corroborate these data, we generated a polyclonal antiserum against the central C2DE domain (Fig 1A), which is the most evolutionary diverse sequence of the protein compared to the other ferlins encoded by *Toxoplasma*. By western blot, the affinity purified antiserum reacts with the full-length FER1 protein with a predicted molecular weight of 159 kDa. In addition, additional bands at approximately 120 and 30 kDa were detected. These bands most likely represent fragments of the full length FER1 protein, although cross reactivity with other proteins cannot be excluded. However, the localization pattern of the α-FER1 serum by IFA resembles the pattern seen with the YFP fusion to the TM domain of FER1, which suggests high specificity for FER1 in IFA (Fig 1D,E). Again, we observe a very apical spot next to a perinuclear signal. To assess whether the perinuclear localization extends beyond the ER we co-stained parasites with dynamin related protein B (DrpB), a marker for the endosome like compartment (ELC) [50]. The ELC is a structure in the secretory pathway past the Golgi apparatus and Trans Golgi Network (TGN) and DrpB is critical for directing microneme and rhoptry proteins to their final destination [50]. Although direct co-staining is weak, the DrpB signal is seen right next to intense FER1 foci (Fig 1D), which suggests they could mark different compartments in the ELC. Together with the continuous perinuclear stain these data indicate that FER1 distributes to the whole secretory pathway including the Golgi apparatus. To elucidate the extreme apical regions to which FER1 localizes we co-stained parasites with antiserum against Vacuole Protein 1 (VP1). VP1 marks the plant like vacuole (PLV) and acidocalcisomes in *Toxoplasma*, but an unspecified apical signal near the conoid is also consistently observed [50-54]. We observe direct co-stain of FER1 and VP1 in the apical tip of the parasite (Fig 1E). Finally, we co-stained extracellular parasites with MIC2 antiserum to highlight the micronemes (Fig 1F). FER1and MIC2 signals were physically distinct, with FER1 more apical than MIC2 in the micronemes. In extracellular parasites, the FER1 signal was more exclusively localizing apical of the nucleus, suggestive of the Golgi, TGN or ELC, contrasting with the peri-nuclear FER1 signal in intracellular parasites and suggesting a dynamic pattern for FER1. Taken together, FER1 localization at the apical VP1 compartment of unknown identity is seen in both intra- and extra-cellular parasites, whereas FER1 marks the entire ER to ELC pathway in intracellular parasites but is absent from the ER in extracellular

bioRxiv preprint doi: https://doi.org/10.1101/2020.04.27.063628; this version posted April 28, 2020. The copyright holder for this preprint (which was not certified by peer review) is the author/funder, who has granted bioRxiv a license to display the preprint in perpetuity. It is made available under aCC-BY-NC-ND 4.0 International license.

parasites. FER1's localization pattern in *T. gondii* is consistent with mammalian ferlins functioning in late endosomal transit versus TGN recycling [41], since trafficking to the rhoptries and micronemes in the Apicomplexa is facilitated by a modified endosomal system [15, 16].

2. Generation and validation of conditionally lethal FER1 mutant lines

To dissect the function of FER1 we followed a dominant negative (DN) approach. We anticipated that conditional overexpression of an allele without the C-terminal TM domain would mislocalize FER1, divert its interacting proteins, and disrupt its function. We generated an α-tubulin promoter driven N-terminal fusion of the destabilization domain (DD) linked to a Myc epitope that can be conditionally stabilized with Shield-1 [55]. We designed both an allele without the 21 C-terminal amino acids encoding the TM domain (DD-Myc-FER1ΔTM) as well as a control construct encoding the full-length FER1 protein (DD-Myc-FER1^{FL}) (Fig 2A). We were able to generate stable parasite lines with both constructs in absence of Shield-1. Expression of the full-length proteins was assessed by western blot, showing higher FER1 levels already in the absence of Shield-1 as the lower MW bands seen in wild type parasites were not observed at the exposure time needed to detect the overexpressed protein (Fig 1C, 2B). Next, we showed by plaque assay that overexpression of both the ΔTM and FL alleles caused a severe fitness defect (Fig 2C). These observations underscore a critical role of FER1 in the lytic cycle as seen in the genome wide CRISPR screen [48].

3. FER1ΔTM overexpression causes a microneme secretion defect

To globally determine the cause of the lethal defect upon FER1ΔTM overexpression we evaluated the following key events of the lytic cycle: host cell invasion (Fig 3A), replication (Fig 3B,C), and host cell egress (Fig 3D-F). Host cell invasion was strongly reduced, consistent with an anticipated FER1 role in invasion through microneme content exocytosis. We observed a mild reduction in the parasite multiplication rate, with a slight but significant (p=0.031) accumulation of parasites in the 4-cells/vacuole stage compared to the controls (Fig 3B). We did not detect a specific delay in a particular cell cycle stage (Fig 3C), suggesting that the overall rate through cell division is somewhat reduced. As summarized in Fig 3D, we triggered egress by several different secretagogues, engaging the signaling pathway toward egress at different points: most upstream is zaprinast to activate protein kinase G (PKG), followed by ethanol activating

bioRxiv preprint doi: https://doi.org/10.1101/2020.04.27.063628; this version posted April 28, 2020. The copyright holder for this preprint (which was not certified by peer review) is the author/funder, who has granted bioRxiv a license to display the preprint in perpetuity. It is made available under aCC-BY-NC-ND 4.0 International license.

phosphoinositide phospholipase C (PI-PLC) right before the bifurcation in a Ca^{2+}-dependent (triggered with Ca^{2+}-ionophore A23187) and phosphatidic acid (PA) dependent pathway (triggered with phosphatidic acid phosphatase (PAP) inhibitor propranolol) [28]. We monitored egress by assessing the integrity of the parasitophorous vacuole membrane (PVM) using GRA3 as PVM marker and the parasite's cytoskeleton marker IMC3 for parasite dispersal in the environment (Fig 3F). None of these secretagogues efficiently induced egress (Fig 3E). To determine whether the defect was specific to egress as observed in CDPK3 signaling mutants [56-58], we permeabilized the plasma membrane with saponin. This bypasses the signaling step specific for egress and triggers the activation of motility by the extracellular environment. Although this did not trigger egress in the FER1ΔTM overexpressing mutant, we noticed loss of PVM integrity upon overexpression. Even though saponin might contribute to this effect, this observation is suggestive of modest microneme release. We performed trail assays as a functional and independent assay to assess microneme secretion, and determined that it is insufficient to support gliding (Fig 3G). Finally, we determined differential microneme secretion from the Rab5A/C-dependent (MIC3, 5, 8) and -independent (MIC2, MIC10, M2AP, PLP1, etc.) microneme sub-populations [9]. The former sub-population was tested by release of processed MIC2 in the medium under various exocytosis triggering conditions, whereas the latter was visualized by MIC3, 5 and 8 protein exposure on the parasite's surface. Overall, we see a sharp reduction in secretion from both microneme populations in the FER1ΔTM overexpressing mutant to nearly undetectable levels. However, we reproducibly detected propranolol induced secretion at a 10-fold lower level than in the non-induced control (a drop from 161% to 15% relative to the total 10% total microneme control; Fig 3H). In addition, we observed a very small amount of MIC3 on the surface of induced parasites, indicating that this population still has minor secretion capacity as well (Fig 3I). Since propranolol triggers the PA pathway, which is independent of the Ca^{2+}-dependent leg (Fig 3D), this section of the pathway appears to be still functioning, albeit at a very low level. Taken together, this suggests that FER1 acts primarily in the Ca^{2+}-dependent events in the micronemal secretory pathway.

4. FER1ΔTM overexpression causes a microneme trafficking defect

By design, we anticipated that FER1ΔTM would mislocalize. Using the Myc-tag in the overexpression DD-Myc-FER1ΔTM construct in IFA revealed a striking accumulate in a defined

bioRxiv preprint doi: https://doi.org/10.1101/2020.04.27.063628; this version posted April 28, 2020. The copyright holder for this preprint (which was not certified by peer review) is the author/funder, who has granted bioRxiv a license to display the preprint in perpetuity. It is made available under aCC-BY-NC-ND 4.0 International license.

mid-apical region, within a background of lower intensity Myc dispersed throughout the cytoplasm also seen in absence of Shield-1 (Fig 4A). We reasoned that the background Myc signal is likely due to proteasome degraded fragments present throughout the cytoplasm. We addressed this concern by overexpressing a YFP version since YFP fragments generated by the proteasome would not autofluorescence. Indeed, we observe no YFP signal without Shield-1 whereas under Shield-1 we see a similar signal in the mid-apical region as seen with the Myc-tagged version. Therefore, we used the YFP version for all subsequent imaging experiments. Co-staining with several microneme proteins in the Rab5A/C-dependent (MIC5 stained) and -independent (MIC2 stained) class showed perfect overlap with the accumulated YFP signal suggesting all microneme proteins are misdirected (Fig 4B,C, S2A,B). The FER1 antiserum signal also co-localizes with the YFP signal. This could suggest that endogenous FER1 may also be diverted from its apical tip and peri-nuclear enrichments to the accumulation of dominant negative FER1ΔTM (Fig 4D), although we cannot rule out the possibility that the massively overexpressed FER1ΔTM as seen by western blot (Fig 2B) overwhelms the endogenous signal. Collectively, these data indicate that both the Rab5A/C dependent and independent microneme sub-populations are controlled by FER1. Since all known microneme protein trafficking mutants in the endosomal sections have concurrent defects in rhoptry protein trafficking [18], we interrogated the rhoptries by IFA. We observed that the ROP proteins remained localized to rhoptries, and that the rhoptries displayed their normal morphology and distribution (Fig 4E). This striking distinction makes the DN-FER1 phenotype a first of its kind for the unique disruption of microneme trafficking while leaving the rhoptries intact.

The central apical localization is reminiscent of the position of various compartments of the *Toxoplasma* secretory pathway. To differentiate whether the accumulation is due to an arrest in trafficking, mis-trafficking, or is of another nature we used a series of secretory pathway specific compartment markers in co-localization experiments (Fig 4F, G). First, we checked whether the FER1 co-localization with PLV/VAC compartment using VP1 as marker. We observe no overlap at all between the VP1 and YFP signals (Fig 4F). We observed similar lack of co-localization with PLV/VAC compartment using NHE3 as an independent marker of this compartment [54] and show that it still displays its normal morphology (Fig S2C). However, we noted that the VP1 signal at the apical end is still very prominent (Fig 4F). Surprisingly, we never observed co-localization of the mid-apical DD-YFP-FER1ΔTM signal with the Golgi

bioRxiv preprint doi: https://doi.org/10.1101/2020.04.27.063628; this version posted April 28, 2020. The copyright holder for this preprint (which was not certified by peer review) is the author/funder, who has granted bioRxiv a license to display the preprint in perpetuity. It is made available under aCC-BY-NC-ND 4.0 International license.

apparatus, TGN, or the ELC, which all displayed their normal morphology. Instead, DD-YFP-FER1ΔTM accumulated in a uncharacterized compartment, beyond any of the known trafficking steps toward the micronemes, and after the split from rhoptry protein trafficking [18].

To reveal the sites of DD-YFP-FER1ΔTM and microneme protein accumulation, we performed transmission electron microscopy (Fig 4H-M). EM studies illustrate that in DD-YFP-FER1ΔTM-expressing parasites, micronemes with normal ultrastructure were not decorating the cytoplasmic side of the cortical cytoskeleton at the apical end but instead were aggregated in the cytoplasm at the apical region of the parasite (Fig 4H). In addition, we observed electron-lucent compartments that in several cases contained electron-dense material (Fig 4I, J). We further investigated the content of these enlarged compartments with possible microneme connection by immunolabeling the parasites with α-MIC2 antibody. Gold particles positioned MIC2 in the aggregated microneme structures (Fig 4K) as well as on the outside edges of the electron-lucent compartments and within the electron-dense spheres within the electron-lucent compartments (Fig 4L,M). The MIC2 association and the appearance of electron dense structures is consistent with the function shared between the ELC and PLV/VAC compartments previously reported [17, 59]. Although these compartments appear enlarged, they are likely part of the physiological trafficking pathways of microneme proteins. In summary, overexpression of dominant negative FER1ΔTM leads to mislocalization of fully mature micronemes without disrupting the trafficking pathway or the biogenesis of the rhoptries. These data indicate that FER1 functions in the trafficking and/or biogenesis of micronemes beyond the ELC, which is the least understood step in microneme biogenesis and secretion [14].

5. DD-YFP-FER1ΔTM overexpression retracts micronemes from the periphery

We tested whether the aggregated micronemes in the mid apical region observed by EM did complete their biogenesis by staining with a marker present on mature micronemes: acylated pleckstrin-homology (PH) domain-containing protein (APH). APH on the microneme's surface senses PA during microneme secretion and is necessary for microneme exocytosis [28]. Indeed, APH co-localized with the site of FER1 accumulation in both intra- and extra-cellular parasites which indicates that the mis-localized micronemes, for signaling purposes, are primed for secretion as in non-induced parasites (Fig 5A). In addition, in extracellular parasites we frequently observed a specific APH signal at the very apical end of the parasite (arrowhead in

bioRxiv preprint doi: https://doi.org/10.1101/2020.04.27.063628; this version posted April 28, 2020. The copyright holder for this preprint (which was not certified by peer review) is the author/funder, who has granted bioRxiv a license to display the preprint in perpetuity. It is made available under aCC-BY-NC-ND 4.0 International license.

Fig 5A). These likely represent a small microneme population that can still be secreted, consistent with the 10% residual microneme secretion in induced parasites (Fig 3H,I). In addition, as guided by the EM data, we asked whether the microneme proteins are fully matured, i.e. completed proteolytic processing by removal of the pro-peptide in the ELC/VAC compartment [17, 20]. We used specific antisera against the pro-peptide of M2AP together with antiserum reacting with the mature M2AP protein [60]. By western blot we observe no difference in relative abundance of the pro-M2AP protein versus the total amount of M2AP protein across all conditions and mutants tested (Fig 5B). Furthermore, by IFA we observe normal MIC5 pro-peptide containing proteins in the ELC compartment [60], and no co-localization with the FER1 accumulation (Fig 5C). These observations further support that the mislocalized micronemes contain mature proteins that completed processing through the secretory pathway.

Since pro-MIC5 manifests predominantly in budding parasites, the co-staining with FER1 revealed another intriguing phenomenon: there appeared to be no DD-YFP-FER1ΔTM accumulation in newly forming parasites. We validated this model by a triple staining with YFP, α-pro-MIC5 and daughter bud marker α-IMC3 (Fig 5D). Moreover, representative images through the division cycle demonstrate that the YFP migrates basally toward the residual body in parasites undergoing division (Fig 5E). Moreover, we never observed any new micronemes in the apical peripherally of daughter buds either (Fig 5F). Collectively, these data indicate that microneme pro-protein processing by the ELC/VAC compartment progresses normally in newly forming daughters, yet new micronemes do not assemble in the daughters, suggesting microneme proteins end up in the YFP-FER1ΔTM pile up formed in the mother. This raised the next intriguing question: is the YFP aggregation independent of cell division? This model implies that normally localized micronemes can be retracted from the periphery and directed toward the YFP microneme aggregate. To this end we performed time courses to determine induction and reversion kinetics of the Shield-1 induced phenotype in both intracellular and extracellular parasites. Microneme mis-localization kinetics were over 95% complete within three hours (Fig 5G top panel). This time frame is much smaller than the 6.5 hr cell division cycle, indicating that the process is not cell cycle dependent as in an unsynchronized population typically 30% of the parasites is undergoing daughter budding [61]. The exact same kinetics were also observed in extracellular parasites which are arrested in a non-division G1/0 state (Fig 5G bottom panel).

bioRxiv preprint doi: https://doi.org/10.1101/2020.04.27.063628; this version posted April 28, 2020. The copyright holder for this preprint (which was not certified by peer review) is the author/funder, who has granted bioRxiv a license to display the preprint in perpetuity. It is made available under aCC-BY-NC-ND 4.0 International license.

What was even more striking is that the phenotype is completely reversible with kinetics very comparator to induction (Fig 5G). Finally, to directly visualize the cell division independent re-localization of the micronemes we performed time lapse microscopy following Shield-1 induction. In DD-YFP-FER1ΔTM co-expressing a MIC3-mCherryRFP marker we observed that microneme retraction and accumulation with YFP-FER1ΔTM started after 1.5 hr of Shield-1 induction (Supplementary Movie S1 and Fig 5H). Moreover, time lapse imaging confirmed that microneme retraction was independent of daughter budding as tracked with a marker enriched in daughter cytoskeletons, IMC3-mCherryRFP (Supplementary Movie S2 and Fig S3). Taken together, overexpression of a dominant negative FER1 allele induces retraction of already correctly localized micronemes from the periphery toward a centrally localized organelle accumulation regardless of cell division cycle stage. The reversible nature of the FER1 mediated process indicates that whole organelle microneme trafficking in principle is bidirectional from where they are docked on the subpellicular micronemes to the site of apical aggregation beyond the known secretory pathway compartments. Therefore, our data reveal that microneme trafficking can in principle be bidirectional and might not be exclusively targeted toward the apical end in support of exocytosis.

6. FER1^{FL} overexpression results in premature, untriggered microneme secretion

The precarious nature of FER1 function was evident from the lethal effect of DD-Myc-FER1^{FL} overexpression (Fig 2C). We dissected this phenotype first by assessing the localization of FER1, which is largely unchanged upon Shield-1 induction and presents on membrane structures throughout the parasite. (Fig 6A). Next, we asked whether these parasites display changes in their microneme secretion ability using the set of secretagogues applied to the ΔTM mutant. We observe strong exocytosis under all conditions, compared to the negative DMSO control (Fig 6B). Although we see slight variations in the sensitivity to different secretagogues compared to the non-induced and wild type parasites (Fig S1), they were not significant and unlikely responsible for the lethal phenotype.

Next, we focused on microneme localization and morphology by IFA. We first assessed the Rab5A/C-dependent sub-population using MIC5 and MIC8 as representatives. In non-induced parasites these display the typical microneme pattern. Upon full-length FER1 overexpression, a dissociation of Rab5A/C-dependent microneme sub-population from the

bioRxiv preprint doi: https://doi.org/10.1101/2020.04.27.063628; this version posted April 28, 2020. The copyright holder for this preprint (which was not certified by peer review) is the author/funder, who has granted bioRxiv a license to display the preprint in perpetuity. It is made available under aCC-BY-NC-ND 4.0 International license.

subpellicular microtubule was observed, but the most apical microneme localization remained (Fig 6C). Staining for the Rab5A/C-independent population with MIC2 again revealed a change in localization pattern, but this was dramatically different from the MIC8 population. By super-resolution SIM, in induced intracellular parasites the microneme signal was strongly concentrated at the apical end, unlike the tapering signal observed in wild type and non-induced controls (Fig 6D top panels). These extremely apical micronemes, also maintained for the Rab5A/C-dependent population, are reminiscent of the radial micronemes organized just below the conoid [12]. The radial micronemes are anchored firmly in the apical region and believed to be primed for secretion [11]. In extracellular parasites however, we did not notice dramatic changes between the induced mutant and the controls: under all conditions MIC2 was more shifted apically compared to the intracellular wild type distribution, yet not so radically apical as in the intracellular induced mutant parasites (Fig 6D lower panels). To obtain an even higher resolution visual on the micronemes in this mutant we resorted to both IEM and TEM. Here we observe an accumulation of micronemes at the apical end, confirming the apical MIC signals seen by light microscopy (Fig 6E, F). Several micronemes were squeezed inside the conoid, whereas the densely packed micronemes in the apical region just below the conoid often displayed an elongated morphology. Further below, we do see scattered micronemes, which likely were the MIC8 micronemes as observed by IFA. Thus, it appears overexpression of N-terminally tagged, full-length FER1 has a differential effect depending on the population of micronemes set apart by Rab5A/C dependence: the MIC2 population is driven to the apical end, whereas the MIC8 population becomes more scattered. Taken together, this is suggestive of a role for FER1 in directing micronemes along the subpellicular microtubules toward the conoid.

To gain further insights in this phenotype we tested specific functional capacities of these apically concentrated micronemes. We first showed that swift parasite egress could be triggered by Shield-1 addition alone (Fig 6I). Egress implies microneme secretion, which we subsequently tested under intracellular conditions in Endo buffer [62]. Release of MIC2, albeit weakly, was observed upon Shield-1 induced egress (Fig 6J). However, we never observed robust levels of MIC2 release, suggesting that only a small pool of micronemes can be released immediately upon Shield-1 treatment. However, already a small amount of micronemal protein release could lead to parasitophorous vacuole membrane permeabilization due to the action of perforin like protein 1 (PLP1) secreted from the micronemes [4]. To further test the FER1 mediated

bioRxiv preprint doi: https://doi.org/10.1101/2020.04.27.063628; this version posted April 28, 2020. The copyright holder for this preprint (which was not certified by peer review) is the author/funder, who has granted bioRxiv a license to display the preprint in perpetuity. It is made available under aCC-BY-NC-ND 4.0 International license.

383 microneme release capacity independent of other signaling triggers we tested whether egress
384 could be triggered in small vacuoles, which have not yet established an acidified PVM [5] or
385 accumulated secreted diacylglycerol kinase 2 (DGK2) inside the PV [63], both of which are
386 required for natural egress [6]. To this end we modified the standard red-green invasion assay
387 into an invasion+egress assay exploiting the same differential staining of intracellular vs
388 extracellular parasites [64]. Following 1 hr standard invasion, non-invaded parasites were
389 washed away and Shield-1 added for two hrs (Fig 6K top). Nearly 50% of vacuoles with single
390 parasites have egressed (Fig 6K bottom), which largely mimics the 60% egress rate seen after 2
391 hrs of induction from large vacuoles. Collectively, these data strongly support that Shield-1
392 induced microneme secretion is only due to FER1 and not due to activation of the generic
393 signaling pathways leading to egress.
394
395 **7. Putative Ca^{2+}-binding residues are critical for FER1 function**
396 To probe the mechanism of FER1 beyond the TM domain we analyzed the individual C2
397 domains for their functional potential. C2 domains fold into β-sheets connected by three loops
398 that can bind to proteins or insert in membranes, which can be modulated upon binding Ca^{2+} [33,
399 34, 38, 39]. Five key residues in the loops, of which the three central ones carry most weight
400 [37], can predict an association with phospholipids in membranes or Ca^{2+}. Across the C2
401 domains in FER1, we only detected Ca^{2+}-binding potential in the C2D domain which carries
402 three Asp residues and a supportive Glu residue in the conserved loop positions which
403 potentially can stabilize two Ca^{2+} ions (Fig 7A,B). We tested the contribution of the C2D domain
404 to FER1 function by mutating two of the conserved Asp residues in loop 1 to Ala, which is
405 predicted to disrupt binding both Ca^{2+} ions (Fig 7B). We conditionally overexpressed the mutant
406 FER1 allele carrying the D541A and D545A mutations in the same N-terminal DD fusion
407 context of a ΔTM or full-length allele. We were unable to express either alleles stably within
408 parasites, even in absence of Shield-1, which indicates that these C2D residues are very critical
409 to FER1 function. Instead we performed transient transfections to analyze the consequences of
410 these mutant alleles on the parasite (Fig 7C, D). Expression levels of the transgenes under
411 Shield-1 were high as vacuoles positive for both Myc and α-FER1 staining clearly stand out in
412 both channels. However, in Myc negative vacuoles the endogenous FER1 was not discernable
413 under the settings used to optimally display the FER1 signal in overexpressing parasites,

bioRxiv preprint doi: https://doi.org/10.1101/2020.04.27.063628; this version posted April 28, 2020. The copyright holder for this preprint (which was not certified by peer review) is the author/funder, who has granted bioRxiv a license to display the preprint in perpetuity. It is made available under aCC-BY-NC-ND 4.0 International license.

indicating that expression of the mutant allele is well above endogenous FER1 levels. Most notable however, the aggregated FER1 signal was not seen upon overexpression of the wild type FER1ΔTM allele, indicating that the C2D domain is critical in mediating this phenotype. Overall, the overexpressed full-length DD-Myc-FER1$^{FL\text{-}(D541A,5D45A)}$ pattern is similar to the wild type allele and localizes to various focal membrane structures.

Subsequently, we used representative antisera to assess both the Rab5A/C-dependent (MIC8) and -independent (MIC2) microneme sub-populations by IFA. For the DD-Myc-FER1ΔTM$^{(D541A,D545A)}$ a difference between the two microneme sub-populations was noticeable: the morphology and intensity of the Rab5A/C independent micronemes were indiscernible in non-transfected parasites (MIC2; yellow circle in Fig 7C). However, the Rab5A/C-dependent micronemes became apically defined and strongly concentrated (MIC8; white circle in Fig 7C). This presentation strongly mimics the pattern seen for overexpression of the full-length wild type allele (Fig 6C). Thus, it appears that the Rab5A/C-dependent micronemes do not need a functional FER1's C2D domain to traffic to the apical conoid region upon FER1 overexpression.

In DD-Myc-FER1$^{FL\text{-}(D541A,D545A)}$ overexpressing parasites we do not observe a difference between the microneme sub-populations by IFA. Interestingly, both microneme populations lose their staining intensity compared to wild type parasites (Fig 7D, white circles). Collectively, this indicates that the conferred function of domains in FER1 can change upon the context of the whole proteins, e.g. by certain domains being present or absent (e.g. TM domain), accessible (e.g. N-terminal fusion) or functional (Ca^{2+}-binding).

Discussion

Our findings and insights are summarized in Fig 8 and support several roles for FER1 in the lytic cycle, 1. Microneme protein trafficking between the ELC to the subpellicular microtubules; 2. Directing the micronemes assembled on the subpellicular microtubules forward to the apical end in extracellular parasites; 3. Transport into the conoid and membrane fusion between the microneme and plasma membranes to facilitate exocytosis; 4. From the bi-directional and completely reversible transport of the micronemes from the subpellicular microtubules to a luminal position we infer that the functional relevance of this feature resides in the recently reported microneme recycling from the mother parasite in daughters under assembly [32]. The

bioRxiv preprint doi: https://doi.org/10.1101/2020.04.27.063628; this version posted April 28, 2020. The copyright holder for this preprint (which was not certified by peer review) is the author/funder, who has granted bioRxiv a license to display the preprint in perpetuity. It is made available under aCC-BY-NC-ND 4.0 International license.

dual localization pattern of endogenous FER1 (Fig 1) together with reports on the connection between localization pattern and human ferlins [41] are consistent with these roles: FER1 in the TGN/ELC is responsible for trafficking to (and from) the anchoring site on the subpellicular microtubules, whereas FER1 in the apical end co-localizing with VP1 facilitates fusion with the plasma membrane. Consistent with the tail-anchored transmembrane model [49, 65], just the TM domain fused to a reporter mimics endogenous FER1 localization. Together with the mis-localizing microneme phenotype upon overexpression of the ΔTM allele, we assert that the TM domain is associated with microneme organelle trafficking. Further support for this interpretation is provided by the vesicular localization in the gametocyte cytoplasm reported for the FER1 ortholog PbFLP in *P. berghei* [47].

The kinetics of microneme mislocalization upon overexpression of the DN ΔTM allele provided additional tantalizing insights. Our extensive marker set together with the ultrastructure established beyond a doubt that the aggregated micronemes are fully mature and contain fully processed proteins. Most importantly, we show that completely mature micronemes at any point in the cell cycle in intracellular parasites as well as in extracellular parasites are released from the subpellicular microtubules and traffic back to a cytoplasmic location apical of known secretory pathway compartments where they aggregate. Although similar appearing microneme pile ups were recently reported upon the disruption of the vacuolar-proton ATPase (v-ATPases) in *Toxoplasma*, they contained microneme proteins from which the pro-peptide had not been cleaved [20] and thus do not represent mature micronemes like we observed. However, these data support the notion that microneme morphology appears to be complete before they traffic toward the subpellicular microtubules. Indeed, trafficking of micronemes from mother to daughters was recently reported as well [32], which further supports the feasibility and a biological function for the retrograde microneme organelle transport we observe. Moreover, the effect we see is specific for the micronemes, unlike most other mutants in the endosomal legs of microneme trafficking, which invariable also affect rhoptry protein trafficking (e.g. [21, 23]). Overall, FER1 provides the first mechanistic insight in the microneme specific trafficking after the trafficking pathway diverges from the upstream route shared with the rhoptries.

Overexpression of the full-length FER1 supports a direct role in membrane fusion in the actual exocytosis. The first piece of evidence is that Shield-1 induction leads to fast egress of parasites in vacuoles (Fig 6I,K). This invariably requires microneme secretion, and we directly

bioRxiv preprint doi: https://doi.org/10.1101/2020.04.27.063628; this version posted April 28, 2020. The copyright holder for this preprint (which was not certified by peer review) is the author/funder, who has granted bioRxiv a license to display the preprint in perpetuity. It is made available under aCC-BY-NC-ND 4.0 International license.

476 detect microneme secretion, albeit modest, under intracellular conditions (Fig 6J). This modest
477 release is sufficient to drive egress, but secretion is not sustained, which requires activation of
478 the complete signaling pathway of secreted micronemes (Fig 6B). Thus excess FER1
479 compensates for other requirements for membrane fusion, such as APH engagement with PA in
480 the plasma membrane [30]. In parallel to other secretory systems [66, 67], we believe that only
481 the primed or so-called readily-releasable microneme pool is released in this mutant, but that
482 additional secretion requires renewed priming (e.g. Ca^{2+}-dependent events such as potential
483 phosphorylation of FER1 [68]), which only occurs when the complete signaling cascade is
484 engaged. The so-called radial micronemes which are accumulated right below the conoid make a
485 good candidate for this readily releasable microneme pool [12, 13]. The radial micronemes are
486 tightly anchored as they were the only set of micronemes remaining upon VPS9 knock-down
487 [11]. However, technically we cannot exclude that only one or two micronemes are present as
488 pre-docked micronemes at the plasma membrane and are engaged to complete fusion with the
489 plasma membrane upon FER1 overexpression.
490 An additional phenomenon observed upon FER1 overexpression is that the MIC2
491 microneme population squeezes into the apical end of the parasite, indicating transport was
492 triggered as well. A similar microneme apical migration phenotype was observed upon knock out
493 of the clathrin adaptor protein AP1, although that was not unique to the micronemes and acted
494 much more widely across many aspects of vesicular trafficking, including cell division [23]. But
495 it indicates that FER1 and AP1 both act in the same pathway that facilitates movement of some
496 micronemes to the apical end of the parasite. Since the AP1 mutant did not lead to microneme
497 secretion, we conclude that the short secretion burst, and apical movement are independent
498 events facilitated by FER1 overexpression. Phenomenologically, we interpret the apical
499 movement as part of the process of secretory vesicle replenishment. By comparison, in mammals
500 a role for otoferlin in replenishment of synaptic vesicles is supported, which mimics this
501 particular function of FER1 in *Toxoplasma* [13, 45, 69].
502 Our data on FER1 indicate that the TM domains is needed to anchor FER1 in early
503 segments of the secretory pathway (ER, Golgi, TGN, ELC). C2 domain analysis of FER1 only
504 pointed at C2D with potential for Ca^{2+} binding and no strong indicators of potential phospholipid
505 binding were identified. Among mammalian ferlins, the C2D domain of otoferlin has been
506 demonstrated directly to bind Ca^{2+} [42] and interacts with MyosinVI [70] to enable vesicle

bioRxiv preprint doi: https://doi.org/10.1101/2020.04.27.063628; this version posted April 28, 2020. The copyright holder for this preprint (which was not certified by peer review) is the author/funder, who has granted bioRxiv a license to display the preprint in perpetuity. It is made available under aCC-BY-NC-ND 4.0 International license.

transport [43]. In general, low Ca^{2+} promotes intramolecular protein-protein interactions among otoferlin C2C, C2D, C2E, and C2F domains, whereas high Ca^{2+} triggers a conformational switch and leads to interaction with phospholipids [43] and SNARE proteins *in vitro* [71, 72]. Translated onto *Toxoplasma* FER1, these observations and our analysis suggest that the C2 domains function in intra-molecular protein-protein interactions to expose or hide functional domains conditional upon signaling conditions. Indeed, depending on the FER1 mutant used, we observe distinct effects on the Rab5A/C-dependent and -independent microneme populations. For example, upon full-length overexpression we observe the Rab5A/C-independent micronemes (MIC2) moving forward without a notable change in the Rab5A/C-dependent micronemes (MIC5/8), whereas without the TM, the C2D Ca^{2+}-binding sites are needed to drive the MIC5/8 micronemes apically, suggesting the TM acts differentially on these microneme subsets. The C2D Ca^{2+}-binding sites promote apical microneme migration along the subpellicular microtubules. In addition, an intact C2D domain is needed to either maintain or form the MIC2 micronemes (we cannot differentiate between these two scenarios). The complex patterns of dynamic and differential changes suggest a model wherein different FER1 domains modulate each other's function dependent on the context: e.g. the C2D domain binds to other C2 domains within the FER1 proteins and stabilizes a certain protein fold consistent with one of FER1's different functions. There are ample signaling events associated with the micronemes that may act to expose, shield, and/or activate other C2 domains in FER1 [6], such as phosphorylation by CDPK1 [73], PKA [7] or PKG [74, 75], binding of DOC2 upon high Ca^{2+} [27] and/or lipids becoming available in the signaling pathway due to PAP activity [28] or the guanylate-cyclase-flippase localized at the apical plasma membrane [63], toward membrane fusion competence.

Incapacitating Ca^{2+}-binding in the C2D domain changes FER1 activity in intracellular parasites which have a low cytoplasmic Ca^{2+} concentration. This suggests that this domain has a high affinity for Ca^{2+}. Given the absence of critical amino acids able to stabilize Ca^{2+} in the other C2 domains, it is unlikely that FER1 bind Ca^{2+} with a low affinity when the signal transduction pathway is engaged. However, in Synaptotagmin-1, a mammalian DOC2 protein, conserved Asp residues in the C2A domain interacts with those in C2B, thereby creating a single Ca^{2+} pocket in the DOC2 domain [76], which might apply to FER1. Alternatively, high Ca^{2+} concentration might be transduced by the soluble TgDOC2 protein, which has also been shown to be critical to microneme secretion [27]. In this scenario, paralleled in neurotransmitter release [77], a raise in

bioRxiv preprint doi: https://doi.org/10.1101/2020.04.27.063628; this version posted April 28, 2020. The copyright holder for this preprint (which was not certified by peer review) is the author/funder, who has granted bioRxiv a license to display the preprint in perpetuity. It is made available under aCC-BY-NC-ND 4.0 International license.

538 cytoplasmic Ca^{2+} would drive TgDOC2 to interact with the membrane fusion complex at the
539 primed, radial micronemes as the critical Ca^{2+}-mediated step in membrane fusion and exocytosis.
540 A caveat from dominant negative allele overexpression studies is that they are generated
541 in presence of an intact endogenous allele. The overexpression of the N-terminally tagged wild-
542 type allele resulted somewhat surprisingly in a cytoplasmic localization. Possibly, the N-terminal
543 fusion blocks functionality requiring an accessible FER1 N-terminus, or alternatively, the high
544 level of overexpression saturates the secretory pathway driving the protein into the cytoplasm.
545 Although the second scenario is supported by the higher level of overexpressed protein
546 compared to the ΔTM allele, where we do not observe a cytoplasmic signal, access to the N-
547 terminus is likely essential as well. We were unable to obtain stable parasite lines where
548 endogenous FER1 was tagged on either the N- or C-terminus. Neither were we able to generate
549 parasite lines with conditional alleles using any of the systems available in *Toxoplasma*
550 (tetracycline regulatable promoter replacement or replacing the 3'-UTR with the conditional U1
551 snRNP motif). Even though a C-terminal tagged PbFLP was stable in *P. berghei* [47], we
552 conclude that in *Toxoplasma* tachyzoites the amenability of FER1 to manipulation has an
553 extremely narrow bandwidth. We successfully bypassed this obstacle by generating antisera
554 against FER1 for localization studies, and the overexpression of dominant negative alleles to
555 determine FER1 function.
556 Another intriguing question generated by our study is the nature of the co-localization of
557 FER1 and VP1 at the apical end. All insights on ferlins in general together with our data suggest
558 that FER1 is microneme associated, which would suggest this signal most likely corresponds
559 with the radial micronemes. Ergo, why is there VP1 in the radial micronemes? VP1 is associated
560 with the acidocalcisomes [78], which it acidifies, as well as with the PLV/VAC [51], where its
561 function is less clear as a distinct v-ATPase acidifies that compartment [20]. This suggests that
562 acidification of the radial micronemes might precede their secretion. Indeed, acidification of the
563 readily releasable vesicle pool is a priming mechanism described in a variety of secretory
564 systems, including neurotransmitter [79] and insulin release [80-82]. In these systems
565 acidification is facilitation by a v-ATPase. Whether VP1 is a functional replacement of this
566 function in *T. gondii* is as yet an untested aspect of this model. Either way, the exact role of the
567 v-ATPase is debated as it has also been shown to act more as a pH sensor [83, 84]. Our
568 observation that VP1 remains apically when all micronemes aggregate upon ΔTM

bioRxiv preprint doi: https://doi.org/10.1101/2020.04.27.063628; this version posted April 28, 2020. The copyright holder for this preprint (which was not certified by peer review) is the author/funder, who has granted bioRxiv a license to display the preprint in perpetuity. It is made available under aCC-BY-NC-ND 4.0 International license.

overexpression could suggest a dynamic composition of this compartment, although we cannot exclude that endogenous FER1 still co-localizes with VP1 under these conditions. This latter scenario fits with our observation that a small pool of micronemes remains sensitive to propranolol induced secretion, which must reside apically to be secreted.

Additional players with related apical localization patterns comprise Rab11a [29]. Depletion of Rab11a reduces motility [85], whereas overexpression of a dominant negative allele reduces MIC2 secretion [29]. But Rab11a's main function is in dense granule secretion with an additional role in cell division [86], which therefore makes its role pleomorphic and complicates to drawing direct connections between Rab11a and FER1 events. Such pluriform role is akin to the defect in microneme apical movement seen upon the knock-out of AP1 [23]. Further strengthening a putative ferlin – Rab11 connection is based on a similar observations for human ferlin Fer1L6, which cycles between the PM and trans-Golgi/recycling endosomes via Rab11 recycling endosomes [41]. Therefore, a connection between *T. gondii's* Rab11a and FER1 at the actual microneme secretion step is quite likely.

Centrin2 is another player at the apical tip of the parasite with multiple additional localizations in the parasite (centrosome, apical annuli, basal complex) that was recently connected to microneme secretion [26, 87]. Furthermore, a centromeric protein, Chromo1, is also present at the same apical localization, but a putative role with microneme secretion has not been explored [23]. Finally, a conserved phosphoinositide-binding protein, PfPH2, was shown in *P. falciparum* to act on a limited set of microneme proteins, although different populations of micronemes have not been demonstrated in *Plasmodium* [88]. Moreover, PfH2 localizes close to the apical tip or merozoites, not unlike where FER1 and VP1 co-localize. The paucity in our understanding of microneme secretion is the putative role of SNARE proteins at the site of exocytosis [18]. Although it has been extensively reported that ferlins interface with SNAREs in membrane fusion [44, 71, 72], auditory hair cells might release vesicles mediated by otoferlin without SNAREs [89]. Furthermore, it has been postulated that fast, Ca^{2+}-dependent exocytosis is inconsistent with the role of SNAREs [90] and some exocytosis in absence of SNAREs is possible [91]. Some neurotransmitter is still released when all relevant SNAREs are depleted [91], and indeed, alternative models for SNARE independent neurotransmitter release have been postulated [90]. Indeed, the multiple C2 domains in ferlins have been proposed to be able to support membrane binding integrating the Ca^{2+}-sensing and membrane fusion events [40, 92]

bioRxiv preprint doi: https://doi.org/10.1101/2020.04.27.063628; this version posted April 28, 2020. The copyright holder for this preprint (which was not certified by peer review) is the author/funder, who has granted bioRxiv a license to display the preprint in perpetuity. It is made available under aCC-BY-NC-ND 4.0 International license.

and as such FER1 might act in absence of SNAREs in *Toxoplasma*. Taken together, a conglomerate of molecular players at the apical end has been identified with roles in microneme exocytosis. Direct links between the observations will be an exciting avenue for future work.

By integrating the new insights generated in this study we propose a model of microneme exocytosis wherein the radial micronemes constitute a readily releasable vesicle pool primed by acidification as shown in Fig 8. Several aspects of this model remain to be tested, and whether it holds up or not, the eclectic collection of molecular players assembling at the site of microneme secretion predict many as yet unanticipated events to be discovered.

Material and Methods

Parasites and host cells

Transgenic derivatives of the RH strain were maintained in human foreskin fibroblasts (HFF) or hTERT immortalized HFF cells as previously described [93]. Parasite transfections and selections use 1 µM pyrimethamine, 20 µM chloramphenicol, 5 µg/ml FUDR, or a combination of 25 mg/ml mycophenolic acid and 50 mg/ml xanthine (MPA/X). All parasite lines were cloned by limiting dilution.

Generation of constructs and parasite lines

All primer sequences are provided in Supplementary Table S1; all plasmids used are provided in Supplementary Table S2. Expression plasmids fusing ddFKBP destabilization domain (DD) with FER1 were generated from tub-DD-Myc-YFP/sagCAT plasmid [55] by replacing YFP with the PCR amplified FER1 CDS (primer pair 1573/1574) by AvrII and XmaI restriction enzymes to generate tub-DD-Myc-FER1^{FL}/sagCAT and in tub DD-YFP-TgNek1-2(MCS)/sagCAT [94]to generate tub-DD-YFP-FER1^{FL}/sagCAT. FER1ΔTM constructs were generated by amplifying a 3' section without TM domain (primer pair 1651/1652; deletion of the C-terminal 21 aa) and cloning the product in the FER1-FL plasmids using NheI and XmaI. The FER1 Ca^{2+}-binding mutants in the C2D domain were generated by Q5 site directed mutagenesis kit (NEB) using primers 4833/4834 to change positions A1622 and A1634 to C resulting in Asp codon 542 and 545 changes to Ala.

bioRxiv preprint doi: https://doi.org/10.1101/2020.04.27.063628; this version posted April 28, 2020. The copyright holder for this preprint (which was not certified by peer review) is the author/funder, who has granted bioRxiv a license to display the preprint in perpetuity. It is made available under aCC-BY-NC-ND 4.0 International license.

Plasmid tub-YFP-FER1(TM) encoding only the 31 most C-terminal aa of FER1 including the TM domain was cloned by PCR amplification using primer pair 4786/4788 and cloned by Gibson assembly into BglII/AvrII digested tub-YFPYFP/sagCAT plasmid [46].

Plasmid tub-IMC3mCherry/DHFR was cloned by swapping IMC3mCherry from tub-IMC3mCherry/sagCAT [95] with PmeI/AvrII into tub-YFPYFP(MCS)/DHFR [46].

To generate pmic3-MIC3-Cherry/DHFR 1.3 kb of promoter region together with 1.2 kb of the ORF encoding genomic locus was PCR amplified from genomic DNA (primer pair 4864/4865) and Gibson assembled into PmeI and AvrII digested tub-mCherry$_2$/DHFR [96].

Antiserum generation

TgFER1 amino acids 669-877 including the diverse C2 domain DE were PCR amplified using primers Ava-LIC-Fer1-F/R and fused to a 6xHis tag in plasmid pAVA0421 [97], expressed in *Escherichia coli* BL21, purified by Ni-NTA chromatography (Invitrogen), and used to immunize a guinea pig (Covance, Inc). Serum was affinity purified as described previously [98] against recombinant His6-TgFER1.

Live-cell microscopy

For monitoring egress (P30-YFP and GCaMP3 expression), parasites were grown in hTERT confluent 15 mm glass bottom cell culture dish (MatTek Corporation, cat #801002) for 30 hrs and then induced with 2 µM Shield-1 for 90 min at 37ºC. Dishes were live-cell imaged on a Zeiss Axiovert 200M inverted microscope for 15 min at 2 images per minute. To monitor DD-YFP-FER1ΔTM accumulation a Leica TCS SP5 scanning confocal microscope with incubation chamber in the Boston College Imaging Core in consultation with Bret Judson. Upon addition of 1 µM Shield-1 images were captured every 5 mins for 3 hrs. All images were acquired, analyzed and adjusted using Leica, Volocity (Quorum Technologies) and/or ImageJ/FIJI software [99, 100].

(Immuno-) fluorescence microscopy

Indirect immunofluorescence assays were performed on intracellular parasites grown for 18 hrs in 6-well plate containing coverslips confluent with HFF cells fixed with 100% methanol (unless stated otherwise) using primary antisera as listed in Supplementary Table S3. Alexa 488 (A488)

bioRxiv preprint doi: https://doi.org/10.1101/2020.04.27.063628; this version posted April 28, 2020. The copyright holder for this preprint (which was not certified by peer review) is the author/funder, who has granted bioRxiv a license to display the preprint in perpetuity. It is made available under aCC-BY-NC-ND 4.0 International license.

or A594 conjugated goat α-mouse, α-rabbit, α-rat, or α-guinea pig were used as secondary antibodies (1:500, Invitrogen). DNA was stained with 4',6-diamidino-2-phenylindole (DAPI). For intracellular IFAs, parasites were allowed to invade and replicate for 24 h after which 1 µM Shield-1 was applied for 18 hr (DD-Myc/YFP-FERΔTM) or 2 µM Shield-1 for 3 hr (DD-Myc-FER^{FL}). Extracellular parasites grown ± Shield-1 for 18 hr were harvested by mechanical lysis and captured on Poly-L-lysine coated coverslips. A Zeiss Axiovert 200 M wide-field fluorescence microscope was used to collect images, which were deconvolved and adjusted for phase contrast using Volocity software). SR- SIM was performed on intracellular parasites fixed with 3.7% or 4% PFA in PBS and permeabilized with 0.25% or 0.5% TX-100 that were imaged with a Zeiss ELYRA S.1 system in the Boston College Imaging Core in consultation with Bret Judson. All images were acquired, analyzed and adjusted using ZEN software and standard settings. Final image analyses were made with ImageJ/FIJI software [99, 100].

Electron microscopy

For ultrastructural observations of *T. gondii*-infected cells by thin-section transmission electron microscopy (TEM), infected cells were fixed in 2.5% glutaraldehyde in 0.1 mM sodium cacodylate (EMS) and processed as described [101]. Ultrathin sections of infected cells were stained before examination with a Philips CM120 EM (Eindhoven, the Netherlands) under 80 kV. For immunoelectron microscopy (IEM) samples were prepared as described before [46]. Sections were immunolabeled with MIC2 MAb 6D10 in 1% fish skin gelatin and then with goat anti-IgG antibodies, followed by 10-nm protein A-gold particles before examination with a Philips CM120 electron microscope under 80 kV.

Host cell invasion

Extracellular parasites from 80% naturally lysed flask were induced with 2 µM Shield-1 for 90 min at 37ºC before they were allowed to invade HFF host cells for 10 min at 37ºC [7]. The red/green invasion assay was performed as described [102] using Alexa594- and Alexa488-conjugated SAG1 MAb T41E5. Three images were taken per biological replicate on an EVOS FL (Life Technologies). The number of invaded versus uninvaded parasites were enumerated manually for at least 300 parasites per counted sample.

bioRxiv preprint doi: https://doi.org/10.1101/2020.04.27.063628; this version posted April 28, 2020. The copyright holder for this preprint (which was not certified by peer review) is the author/funder, who has granted bioRxiv a license to display the preprint in perpetuity. It is made available under aCC-BY-NC-ND 4.0 International license.

Secretagogue induced egress

The egress assay was performed essentially as described previously [46]. Parasites were grown in HFF monolayers for 30 h after which the phenotype was induced with 1 µM Shield-1 for 18 hrs. Egress was triggered with 1-3 µM A23187, 500 µM propranolol, 50-150 µM BIPPO (kindly shared by Dr. Jeff Dvorin) 0.01-0.1% saponin or DMSO for 5 min at 37°C, followed by IFA with IMC3 and GRA3 antisera. Egressed, permeabilized and intact vacuoles were counted [63]. 100 vacuoles were counted for each experiment and three biological replicates were performed.

Shield-1 induced egress

Parasites were inoculated on HFF coverslips and allowed to grow for 30 hrs and then induced with either 1 µM Shield-1 for 2 hrs or 1 µM calcium ionophore A23187 for 5 min as a control, prior to fixation with 100% methanol and IFA staining using MAb 9E10 cMyc and rabbit αMIC8 (antisera details in Supplementary Table S1). DNA was stained with 4',6-diamidino-2-phenylindole (DAPI). The number of intact vacuoles per 20 fields was enumerated.

Combined invasion-egress Assay

Parasites were grown for 36 hours, mechanically lysed in standard ED1 parasite medium and allowed to invade coverslips coated in an HFF monolayer for 1 hr. All unattached parasites were then washed off with a PBS and coverslips were incubated in 1 µM Shield-1 or vehicle control for an additional 2 hrs. Coverslips were then fixed with PFA and IFA was performed as described for a typical red-green invasion assay.

Shield-1 induced microneme secretion

Parasites were grown for 30 hrs in a T25 hTERT containing flask. Flasks were washed once with PBS and once with Endo buffer (20 mM Tris-H_2SO_4 pH 8.2, 44.7 mM K_2SO_4, 106 mM sucrose, 3.5 mg/ml BSA,10 mM $MgSO_4$) [62]. Cells were scraped and parasites mechanically released. Parasites pellets were re-suspended in Endo buffer and treated with either 1 µM Shield-1 for 2 hrs or A23187 for 5 min prior to processing. All other secretion steps are as previously stated. Supernatants were processed for western blot.

Microneme secretion by Western blotting

bioRxiv preprint doi: https://doi.org/10.1101/2020.04.27.063628; this version posted April 28, 2020. The copyright holder for this preprint (which was not certified by peer review) is the author/funder, who has granted bioRxiv a license to display the preprint in perpetuity. It is made available under aCC-BY-NC-ND 4.0 International license.

Microneme secretion by western blot was performed as published [103]. Freshly lysed parasites were resuspended in DMEM/FBS and transferred to a 96-well polystyrene round-bottom plate (CELLTREAT Scientific Products). Secretion was induced by 1-3 µM A23187, 500 µM propranolol, 1% ethanol or DMSO for 5 min at 37°C. Constitutive microneme secretion was assessed by incubation without secretagogue at 37°C for 60 min. Supernatants were probed by western blot using 6D10 MIC2 MAb and TG17.43 GRA1 MAb and HRP conjugated secondary antiserum. Signals were quantified using a densitometer.

Microneme secretion by IFA

IFA on parasites exposed to a host cell monolayer was performed as reported [46]. Parasites were resuspended in Endo buffer and spun onto HFF cells in a 6-well plate at 28*g, 5 min, RT and allowed to settle for 20 min at 37°C. Secretion was induced by replacing the buffer with 3% FBS in DMEM and 10 mM HEPES (pH 7.2) and incubation at 37°C for 5 min. PBS-washed coverslips were fixed with 4% formaldehyde and 0.02% glutaraldehyde, and subjected to IFA with anti-Mic3, -Mic5, -Mic8 or Mic10 in the presence of 0.02% saponin.

Gliding motility trail assay

Trail assays were performed as previously described [22]. Parasites were induced with 1 µM Shield-1 for 18 hr, mechanically released, resuspended in ED1 with 1 µM Shield-1 and incubated on poly-L-lysine coated coverslips for 15 min at 37°C. Parasites were fixed with 4% formaldehyde and 0.02% glutaraldehyde and stained with DG52 SAG1 MAb (64) to visualize trails.

Statistics.

Student's paired t test and one-way analysis of variance (ANOVA) using post hoc Bonferroni correction were performed.

Acknowledgements

We thank Bret Judson and Dr. Patrick Autissier of the Boston College Imaging and Flow Cytometry Cores, respectively, for infrastructure and support, Dr. Sander Groffen for assistance

bioRxiv preprint doi: https://doi.org/10.1101/2020.04.27.063628; this version posted April 28, 2020. The copyright holder for this preprint (which was not certified by peer review) is the author/funder, who has granted bioRxiv a license to display the preprint in perpetuity. It is made available under aCC-BY-NC-ND 4.0 International license.

with molecular modeling, Emily Stoneburner, Natalie Sandlin, and Elizabeth Gray for technical support, Drs. Gustavo Arrizabalaga, Peter Bradley, Vern Carruthers, Iain Cheeseman, Jean-François Dubremetz, Wassim Daher, Jeff Dvorin, Maryse Lebrun, Sebastian Lourido, Sabrina Marion, Silvia Moreno, Naomi Morrissette, Jeroen Saeij, David Sibley, Dominique Soldati-Favre, and Gary Ward for sharing reagents.

This study was supported by National Science Foundation (NSF) Major Research Instrumentation grant 1626072, National Institutes of Health grants AI108251 (B.I.C.), AI060767 (I.C.), AI122042 (M.-J.G), AI099658 (M.-J.G.), and AI122923 (M.-J.G.), and American Cancer Society grant RSG-12-175-01-MPC (M.-J.G.).

Author contributions

DNAT performed all experiments on the DD-[Myc/YFP]-FER1ΔTM parasites, imaging of the DD-Myc-FER1^{FL} line, all time lapse and super resolution microscopy and generated and assessed the Asp-Ala mutants, AAD performed all functional studies on the DD-Myc-FER1^{FL} parasites, IC performed all electron microscopy studies, BIC cloned FER1 cDNA, established the overexpression plasmids and assessed the initial phenotype, DNAT, AAD and MJG designed the experiments and interpreted the data, MJG wrote the manuscript and all authors reviewed and edited the manuscript.

Conflict of interest

The authors declare no conflict of interest.

References

1. Blader, I.J., B.I. Coleman, C.T. Chen, and M.J. Gubbels, 2015. *Lytic Cycle of Toxoplasma gondii: 15 Years Later.* Annu Rev Microbiol, 69: 463-85.
2. Carruthers, V.B. and F.M. Tomley, 2008. *Microneme proteins in apicomplexans.* Subcell Biochem, 47: 33-45.
3. Sheiner, L., J.M. Santos, N. Klages, F. Parussini, N. Jemmely, N. Friedrich, G.E. Ward, and D. Soldati-Favre, 2010. *Toxoplasma gondii transmembrane microneme proteins and their modular design.* Mol Microbiol.
4. Kafsack, B.F., J.D. Pena, I. Coppens, S. Ravindran, J.C. Boothroyd, and V.B. Carruthers, 2009. *Rapid membrane disruption by a perforin-like protein facilitates parasite exit from host cells.* Science, 323: 530-3.

bioRxiv preprint doi: https://doi.org/10.1101/2020.04.27.063628; this version posted April 28, 2020. The copyright holder for this preprint (which was not certified by peer review) is the author/funder, who has granted bioRxiv a license to display the preprint in perpetuity. It is made available under aCC-BY-NC-ND 4.0 International license.

5. Roiko, M.S., N. Svezhova, and V.B. Carruthers, 2014. *Acidification Activates Toxoplasma gondii Motility and Egress by Enhancing Protein Secretion and Cytolytic Activity.* PLoS Pathog, 10: e1004488.
6. Bullen, H.E., H. Bisio, and D. Soldati-Favre, 2019. *The triumvirate of signaling molecules controlling Toxoplasma microneme exocytosis: Cyclic GMP, calcium, and phosphatidic acid.* PLoS Pathog, 15: e1007670.
7. Uboldi, A.D., M.L. Wilde, E.A. McRae, R.J. Stewart, L.F. Dagley, L. Yang, N.J. Katris, S.V. Hapuarachchi, M.J. Coffey, A.M. Lehane, C.Y. Botte, R.F. Waller, A.I. Webb, M.J. McConville, and C.J. Tonkin, 2018. *Protein kinase A negatively regulates Ca2+ signalling in Toxoplasma gondii.* PLoS Biol, 16: e2005642.
8. Leung, J.M., Y. He, F. Zhang, Y.C. Hwang, E. Nagayasu, J. Liu, J.M. Murray, and K. Hu, 2017. *Stability and function of a putative microtubule-organizing center in the human parasite Toxoplasma gondii.* Mol Biol Cell, 28: 1361-1378.
9. Kremer, K., D. Kamin, E. Rittweger, J. Wilkes, H. Flammer, S. Mahler, J. Heng, C.J. Tonkin, G. Langsley, S.W. Hell, V.B. Carruthers, D.J. Ferguson, and M. Meissner, 2013. *An overexpression screen of Toxoplasma gondii Rab-GTPases reveals distinct transport routes to the micronemes.* PLoS Pathog, 9: e1003213.
10. Jacot, D., N. Tosetti, I. Pires, J. Stock, A. Graindorge, Y.F. Hung, H. Han, R. Tewari, I. Kursula, and D. Soldati-Favre, 2016. *An Apicomplexan Actin-Binding Protein Serves as a Connector and Lipid Sensor to Coordinate Motility and Invasion.* Cell Host Microbe, 20: 731-743.
11. Sakura, T., F. Sindikubwabo, L.K. Oesterlin, H. Bousquet, C. Slomianny, M.A. Hakimi, G. Langsley, and S. Tomavo, 2016. *A Critical Role for Toxoplasma gondii Vacuolar Protein Sorting VPS9 in Secretory Organelle Biogenesis and Host Infection.* Scientific Reports, 6.
12. Paredes-Santos, T.C., W. de Souza, and M. Attias, 2012. *Dynamics and 3D organization of secretory organelles of Toxoplasma gondii.* Journal of structural biology, 177: 420-30.
13. Saha, S., B.I. Coleman, R. Dubey, I.J. Blader, and M.J. Gubbels, 2017. *Two Phosphoglucomutase Paralogs Facilitate Ionophore-Triggered Secretion of the Toxoplasma Micronemes.* mSphere, 2.
14. Venugopal, K. and S. Marion, 2018. *Secretory organelle trafficking in Toxoplasma gondii: A long story for a short travel.* Int J Med Microbiol, 308: 751-760.
15. Sangare, L.O., T.D. Alayi, B. Westermann, A. Hovasse, F. Sindikubwabo, I. Callebaut, E. Werkmeister, F. Lafont, C. Slomianny, M.A. Hakimi, A. Van Dorsselaer, C. Schaeffer-Reiss, and S. Tomavo, 2016. *Unconventional endosome-like compartment and retromer complex in Toxoplasma gondii govern parasite integrity and host infection.* Nat Commun, 7: 11191.
16. Tomavo, S., C. Slomianny, M. Meissner, and V.B. Carruthers, 2013. *Protein trafficking through the endosomal system prepares intracellular parasites for a home invasion.* PLoS Pathog, 9: e1003629.
17. Thornton, L.B., P. Teehan, K. Floyd, C. Cochrane, A. Bergmann, B. Riegel, A.J. Stasic, M. Di Cristina, S.N.J. Moreno, P.D. Roepe, and Z. Dou, 2019. *An ortholog of Plasmodium falciparum chloroquine resistance transporter (PfCRT) plays a key role in maintaining the integrity of the endolysosomal system in Toxoplasma gondii to facilitate host invasion.* PLoS Pathog, 15: e1007775.

bioRxiv preprint doi: https://doi.org/10.1101/2020.04.27.063628; this version posted April 28, 2020. The copyright holder for this preprint (which was not certified by peer review) is the author/funder, who has granted bioRxiv a license to display the preprint in perpetuity. It is made available under aCC-BY-NC-ND 4.0 International license.

18. Dubois, D.J. and D. Soldati-Favre, 2019. *Biogenesis and secretion of micronemes in Toxoplasma gondii.* Cell Microbiol, 21: e13018.
19. McGovern, O.L., Y. Rivera-Cuevas, G. Kannan, A.J. Narwold, and V.B. Carruthers, 2018. *Intersection of endocytic and exocytic systems in Toxoplasma gondii.* Traffic, 19: 336-353.
20. Stasic, A.J., N.M. Chasen, E.J. Dykes, S.A. Vella, B. Asady, V.J. Starai, and S.N.J. Moreno, 2019. *The Toxoplasma Vacuolar H(+)-ATPase Regulates Intracellular pH and Impacts the Maturation of Essential Secretory Proteins.* Cell Rep, 27: 2132-2146 e7.
21. Sloves, P.J., S. Delhaye, T. Mouveaux, E. Werkmeister, C. Slomianny, A. Hovasse, T. Dilezitoko Alayi, I. Callebaut, R.Y. Gaji, C. Schaeffer-Reiss, A. Van Dorsselear, V.B. Carruthers, and S. Tomavo, 2012. *Toxoplasma sortilin-like receptor regulates protein transport and is essential for apical secretory organelle biogenesis and host infection.* Cell Host Microbe, 11: 515-27.
22. Morlon-Guyot, J., S. Pastore, L. Berry, M. Lebrun, and W. Daher, 2015. *Toxoplasma gondii Vps11, a subunit of HOPS and CORVET tethering complexes, is essential for the biogenesis of secretory organelles.* Cellular Microbiology.
23. Venugopal, K., E. Werkmeister, N. Barois, J.M. Saliou, A. Poncet, L. Huot, F. Sindikubwabo, M.A. Hakimi, G. Langsley, F. Lafont, and S. Marion, 2017. *Dual role of the Toxoplasma gondii clathrin adaptor AP1 in the sorting of rhoptry and microneme proteins and in parasite division.* PLoS Pathog, 13: e1006331.
24. Bradley, P.J. and J.C. Boothroyd, 2001. *The pro region of Toxoplasma ROP1 is a rhoptry-targeting signal.* Int J Parasitol, 31: 1177-86.
25. Bradley, P.J., N. Li, and J.C. Boothroyd, 2004. *A GFP-based motif-trap reveals a novel mechanism of targeting for the Toxoplasma ROP4 protein.* Mol Biochem Parasitol, 137: 111-20.
26. Lentini, G., D.J. Dubois, B. Maco, D. Soldati-Favre, and K. Frenal, 2019. *The roles of Centrin 2 and Dynein Light Chain 8a in apical secretory organelles discharge of Toxoplasma gondii.* Traffic.
27. Farrell, A., S. Thirugnanam, A. Lorestani, J.D. Dvorin, K.P. Eidell, D.J. Ferguson, B.R. Anderson-White, M.T. Duraisingh, G.T. Marth, and M.J. Gubbels, 2012. *A DOC2 protein identified by mutational profiling is essential for apicomplexan parasite exocytosis.* Science, 335: 218-21.
28. Bullen, H.E., Y. Jia, Y. Yamaryo-Botte, H. Bisio, O. Zhang, N.K. Jemelin, J.B. Marq, V. Carruthers, C.Y. Botte, and D. Soldati-Favre, 2016. *Phosphatidic Acid-Mediated Signaling Regulates Microneme Secretion in Toxoplasma.* Cell Host Microbe, 19: 349-60.
29. Venugopal, K., S. Chehade, E. Werkmeister, N. Barois, J. Periz, F. Lafont, I. Tardieux, J. Khalife, G. Langsley, M. Meissner, and S. Marion, 2019. *Rab11A regulates the constitutive secretory pathway during Toxoplasma gondii invasion of host cells and parasite replication.* bioRxiv.
30. Bullen, H.E. and D. Soldati-Favre, 2016. *A central role for phosphatidic acid as a lipid mediator of regulated exocytosis in apicomplexa.* FEBS Lett, 590: 2469-81.
31. Gras, S., E. Jimenez-Ruiz, C.M. Klinger, K. Schneider, A. Klingl, L. Lemgruber, and M. Meissner, 2019. *An endocytic-secretory cycle participates in Toxoplasma gondii in motility.* PLoS Biol, 17: e3000060.

bioRxiv preprint doi: https://doi.org/10.1101/2020.04.27.063628; this version posted April 28, 2020. The copyright holder for this preprint (which was not certified by peer review) is the author/funder, who has granted bioRxiv a license to display the preprint in perpetuity. It is made available under aCC-BY-NC-ND 4.0 International license.

32. Periz, J., M. Del Rosario, A. McStea, S. Gras, C. Loney, L. Wang, M.L. Martin-Fernandez, and M. Meissner, 2019. *A highly dynamic F-actin network regulates transport and recycling of micronemes in Toxoplasma gondii vacuoles.* Nat Commun, 10: 4183.
33. Martens, S. and H.T. McMahon, 2008. *Mechanisms of membrane fusion: disparate players and common principles.* Nat Rev Mol Cell Biol, 9: 543-56.
34. Martens, S., 2010. *Role of C2 domain proteins during synaptic vesicle exocytosis.* Biochem Soc Trans, 38: 213-6.
35. Corbalan-Garcia, S. and J.C. Gomez-Fernandez, 2014. *Signaling through C2 domains: more than one lipid target.* Biochim Biophys Acta, 1838: 1536-47.
36. Striegel, A.R., L.M. Biela, C.S. Evans, Z. Wang, J.B. Delehoy, R.B. Sutton, E.R. Chapman, and N.E. Reist, 2012. *Calcium binding by synaptotagmin's C2A domain is an essential element of the electrostatic switch that triggers synchronous synaptic transmission.* J Neurosci, 32: 1253-60.
37. Davis, D.B., K.R. Doherty, A.J. Delmonte, and E.M. McNally, 2002. *Calcium-sensitive phospholipid binding properties of normal and mutant ferlin C2 domains.* J Biol Chem, 277: 22883-8.
38. Verdaguer, N., S. Corbalan-Garcia, W.F. Ochoa, I. Fita, and J.C. Gomez-Fernandez, 1999. *Ca(2+) bridges the C2 membrane-binding domain of protein kinase Calpha directly to phosphatidylserine.* EMBO J, 18: 6329-38.
39. Chapman, E.R. and A.F. Davis, 1998. *Direct interaction of a Ca2+-binding loop of synaptotagmin with lipid bilayers.* J Biol Chem, 273: 13995-4001.
40. Lek, A., F.J. Evesson, R.B. Sutton, K.N. North, and S.T. Cooper, 2012. *Ferlins: regulators of vesicle fusion for auditory neurotransmission, receptor trafficking and membrane repair.* Traffic, 13: 185-94.
41. Redpath, G.M., R.A. Sophocleous, L. Turnbull, C.B. Whitchurch, and S.T. Cooper, 2016. *Ferlins Show Tissue-Specific Expression and Segregate as Plasma Membrane/Late Endosomal or Trans-Golgi/Recycling Ferlins.* Traffic, 17: 245-66.
42. Roux, I., S. Safieddine, R. Nouvian, M. Grati, M.C. Simmler, A. Bahloul, I. Perfettini, M. Le Gall, P. Rostaing, G. Hamard, A. Triller, P. Avan, T. Moser, and C. Petit, 2006. *Otoferlin, defective in a human deafness form, is essential for exocytosis at the auditory ribbon synapse.* Cell, 127: 277-89.
43. Pangrsic, T., E. Reisinger, and T. Moser, 2012. *Otoferlin: a multi-C2 domain protein essential for hearing.* Trends in neurosciences, 35: 671-80.
44. Hams, N., M. Padmanarayana, W. Qiu, and C.P. Johnson, 2017. *Otoferlin is a multivalent calcium-sensitive scaffold linking SNAREs and calcium channels.* Proc Natl Acad Sci U S A, 114: 8023-8028.
45. Michalski, N., J.D. Goutman, S.M. Auclair, J. Boutet de Monvel, M. Tertrais, A. Emptoz, A. Parrin, S. Nouaille, M. Guillon, M. Sachse, D. Ciric, A. Bahloul, J.P. Hardelin, R.B. Sutton, P. Avan, S.S. Krishnakumar, J.E. Rothman, D. Dulon, S. Safieddine, and C. Petit, 2017. *Otoferlin acts as a Ca(2+) sensor for vesicle fusion and vesicle pool replenishment at auditory hair cell ribbon synapses.* Elife, 6.
46. Coleman, B.I., S. Saha, S. Sato, K. Engelberg, D.J.P. Ferguson, I. Coppens, M. Lodoen, and M.-J. Gubbels, 2018. *A member of the ferlin calcium sensor family is essential for Toxoplasma gondii rhoptry secretion.* mBio, 9: e01510-18.

bioRxiv preprint doi: https://doi.org/10.1101/2020.04.27.063628; this version posted April 28, 2020. The copyright holder for this preprint (which was not certified by peer review) is the author/funder, who has granted bioRxiv a license to display the preprint in perpetuity. It is made available under aCC-BY-NC-ND 4.0 International license.

47. Obrova, K., M. Cyrklaff, R. Frank, G.R. Mair, and A.K. Mueller, 2018. *Transmission of the malaria parasite requires ferlin for gamete egress from the red blood cell.* Cell Microbiol: e12999.
48. Sidik, S.M., D. Huet, S.M. Ganesan, M.H. Huynh, T. Wang, A.S. Nasamu, P. Thiru, J.P. Saeij, V.B. Carruthers, J.C. Niles, and S. Lourido, 2016. *A Genome-wide CRISPR Screen in Toxoplasma Identifies Essential Apicomplexan Genes.* Cell, 166: 1423-1435 e12.
49. Padgett, L.R., G. Arrizabalaga, and W.J. Sullivan, Jr., 2017. *Targeting of tail-anchored membrane proteins to subcellular organelles in Toxoplasma gondii.* Traffic, 18: 149-158.
50. Breinich, M.S., D.J. Ferguson, B.J. Foth, G.G. van Dooren, M. Lebrun, D.V. Quon, B. Striepen, P.J. Bradley, F. Frischknecht, V.B. Carruthers, and M. Meissner, 2009. *A Dynamin Is Required for the Biogenesis of Secretory Organelles in Toxoplasma gondii.* Curr Biol, 19: 277-86.
51. Miranda, K., D.A. Pace, R. Cintron, J.C. Rodrigues, J. Fang, A. Smith, P. Rohloff, E. Coelho, F. de Haas, W. de Souza, I. Coppens, L.D. Sibley, and S.N. Moreno, 2010. *Characterization of a novel organelle in Toxoplasma gondii with similar composition and function to the plant vacuole.* Mol Microbiol, 76: 1358-75.
52. Drozdowicz, Y.M., M. Shaw, M. Nishi, B. Striepen, H.A. Liwinski, D.S. Roos, and P.A. Rea, 2003. *Isolation and characterization of TgVP1, a type I vacuolar H+-translocating pyrophosphatase from Toxoplasma gondii. The dynamics of its subcellular localization and the cellular effects of a diphosphonate inhibitor.* J Biol Chem, 278: 1075-85.
53. Luo, S., F.A. Ruiz, and S.N. Moreno, 2005. *The acidocalcisome Ca2+-ATPase (TgA1) of Toxoplasma gondii is required for polyphosphate storage, intracellular calcium homeostasis and virulence.* Mol Microbiol, 55: 1034-45.
54. Francia, M.E., S. Wicher, D.A. Pace, J. Sullivan, S.N. Moreno, and G. Arrizabalaga, 2011. *A Toxoplasma gondii protein with homology to intracellular type Na(+)/H(+) exchangers is important for osmoregulation and invasion.* Exp Cell Res.
55. Herm-Gotz, A., C. Agop-Nersesian, S. Munter, J.S. Grimley, T.J. Wandless, F. Frischknecht, and M. Meissner, 2007. *Rapid control of protein level in the apicomplexan Toxoplasma gondii.* Nat Methods, 4: 1003-5.
56. Garrison, E., M. Treeck, E. Ehret, H. Butz, T. Garbuz, B.P. Oswald, M. Settles, J. Boothroyd, and G. Arrizabalaga, 2012. *A forward genetic screen reveals that calcium-dependent protein kinase 3 regulates egress in Toxoplasma.* PLoS Pathog, 8: e1003049.
57. Lourido, S., K. Tang, and L.D. Sibley, 2012. *Distinct signalling pathways control Toxoplasma egress and host-cell invasion.* Embo J, 31: 4524-34.
58. McCoy, J.M., L. Whitehead, G.G. van Dooren, and C.J. Tonkin, 2012. *TgCDPK3 Regulates Calcium-Dependent Egress of Toxoplasma gondii from Host Cells.* PLoS Pathog, 8: e1003066.
59. Parussini, F., I. Coppens, P.P. Shah, S.L. Diamond, and V.B. Carruthers, 2010. *Cathepsin L occupies a vacuolar compartment and is a protein maturase within the endo/exocytic system of Toxoplasma gondii.* Mol Microbiol, 76: 1340-57.
60. Brydges, S.D., J.M. Harper, F. Parussini, I. Coppens, and V.B. Carruthers, 2008. *A transient forward-targeting element for microneme-regulated secretion in Toxoplasma gondii.* Biology of the Cell, 100: 253-264.
61. Nishi, M., K. Hu, J.M. Murray, and D.S. Roos, 2008. *Organellar dynamics during the cell cycle of Toxoplasma gondii.* J Cell Sci, 121: 1559-1568.

bioRxiv preprint doi: https://doi.org/10.1101/2020.04.27.063628; this version posted April 28, 2020. The copyright holder for this preprint (which was not certified by peer review) is the author/funder, who has granted bioRxiv a license to display the preprint in perpetuity. It is made available under aCC-BY-NC-ND 4.0 International license.

62. Endo, T. and K. Yagita, 1990. *Effect of extracellular ions on motility and cell entry in Toxoplasma gondii.* J Protozool, 37: 133-8.
63. Bisio, H., M. Lunghi, M. Brochet, and D. Soldati-Favre, 2019. *Phosphatidic acid governs natural egress in Toxoplasma gondii via a guanylate cyclase receptor platform.* Nat Microbiol, 4: 420-428.
64. Kafsack, B.F., C. Beckers, and V.B. Carruthers, 2004. *Synchronous invasion of host cells by Toxoplasma gondii.* Mol Biochem Parasitol, 136: 309-11.
65. Vogl, C., I. Panou, G. Yamanbaeva, C. Wichmann, S.J. Mangosing, F. Vilardi, A.A. Indzhykulian, T. Pangrsic, R. Santarelli, M. Rodriguez-Ballesteros, T. Weber, S. Jung, E. Cardenas, X. Wu, S.M. Wojcik, K.Y. Kwan, I. Del Castillo, B. Schwappach, N. Strenzke, D.P. Corey, S.Y. Lin, and T. Moser, 2016. *Tryptophan-rich basic protein (WRB) mediates insertion of the tail-anchored protein otoferlin and is required for hair cell exocytosis and hearing.* EMBO J, 35: 2536-2552.
66. Kaeser, P.S. and W.G. Regehr, 2014. *Molecular mechanisms for synchronous, asynchronous, and spontaneous neurotransmitter release.* Annu Rev Physiol, 76: 333-63.
67. Kaeser, P.S. and W.G. Regehr, 2017. *The readily releasable pool of synaptic vesicles.* Curr Opin Neurobiol, 43: 63-70.
68. Meese, S., A.P. Cepeda, F. Gahlen, C.M. Adams, R. Ficner, A.J. Ricci, S. Heller, E. Reisinger, and M. Herget, 2017. *Activity-Dependent Phosphorylation by CaMKIIdelta Alters the Ca(2+) Affinity of the Multi-C2-Domain Protein Otoferlin.* Front Synaptic Neurosci, 9: 13.
69. Pangrsic, T., L. Lasarow, K. Reuter, H. Takago, M. Schwander, D. Riedel, T. Frank, L.M. Tarantino, J.S. Bailey, N. Strenzke, N. Brose, U. Muller, E. Reisinger, and T. Moser, 2010. *Hearing requires otoferlin-dependent efficient replenishment of synaptic vesicles in hair cells.* Nat Neurosci, 13: 869-76.
70. Heidrych, P., U. Zimmermann, S. Kuhn, C. Franz, J. Engel, S.V. Duncker, B. Hirt, C.M. Pusch, P. Ruth, M. Pfister, W. Marcotti, N. Blin, and M. Knipper, 2009. *Otoferlin interacts with myosin VI: implications for maintenance of the basolateral synaptic structure of the inner hair cell.* Hum Mol Genet, 18: 2779-90.
71. Ramakrishnan, N.A., M.J. Drescher, B.J. Morley, P.M. Kelley, and D.G. Drescher, 2014. *Calcium regulates molecular interactions of otoferlin with soluble NSF attachment protein receptor (SNARE) proteins required for hair cell exocytosis.* J Biol Chem, 289: 8750-66.
72. Johnson, C.P. and E.R. Chapman, 2010. *Otoferlin is a calcium sensor that directly regulates SNARE-mediated membrane fusion.* J Cell Biol, 191: 187-97.
73. Lourido, S., J. Shuman, C. Zhang, K.M. Shokat, R. Hui, and L.D. Sibley, 2010. *Calcium-dependent protein kinase 1 is an essential regulator of exocytosis in Toxoplasma.* Nature, 465: 359-62.
74. Donald, R.G. and P.A. Liberator, 2002. *Molecular characterization of a coccidian parasite cGMP dependent protein kinase.* Mol Biochem Parasitol, 120: 165-75.
75. Jia, Y., J.B. Marq, H. Bisio, D. Jacot, C. Mueller, L. Yu, J. Choudhary, M. Brochet, and D. Soldati-Favre, 2017. *Crosstalk between PKA and PKG controls pH-dependent host cell egress of Toxoplasma gondii.* EMBO J.

bioRxiv preprint doi: https://doi.org/10.1101/2020.04.27.063628; this version posted April 28, 2020. The copyright holder for this preprint (which was not certified by peer review) is the author/funder, who has granted bioRxiv a license to display the preprint in perpetuity. It is made available under aCC-BY-NC-ND 4.0 International license.

76. Evans, C.S., Z. He, H. Bai, X. Lou, P. Jeggle, R.B. Sutton, J.M. Edwardson, and E.R. Chapman, 2016. *Functional analysis of the interface between the tandem C2 domains of synaptotagmin-1.* Mol Biol Cell, 27: 979-89.
77. Shin, O.H., 2014. *Exocytosis and synaptic vesicle fusion.* Comprehensive Physiology, 4: 149-175.
78. Luo, S., M. Vieira, J. Graves, L. Zhong, and S.N. Moreno, 2001. *A plasma membrane-type Ca(2+)-ATPase co-localizes with a vacuolar H(+)-pyrophosphatase to acidocalcisomes of Toxoplasma gondii.* EMBO J, 20: 55-64.
79. Morel, N. and S. Poea-Guyon, 2015. *The membrane domain of vacuolar H(+)ATPase: a crucial player in neurotransmitter exocytotic release.* Cell Mol Life Sci, 72: 2561-73.
80. Morel, N., J.C. Dedieu, and J.M. Philippe, 2003. *Specific sorting of the a1 isoform of the V-H+ATPase a subunit to nerve terminals where it associates with both synaptic vesicles and the presynaptic plasma membrane.* J Cell Sci, 116: 4751-62.
81. Rorsman, P. and E. Renstrom, 2003. *Insulin granule dynamics in pancreatic beta cells.* Diabetologia, 46: 1029-45.
82. Barg, S., P. Huang, L. Eliasson, D.J. Nelson, S. Obermuller, P. Rorsman, F. Thevenod, and E. Renstrom, 2001. *Priming of insulin granules for exocytosis by granular Cl(-) uptake and acidification.* J Cell Sci, 114: 2145-54.
83. Poea-Guyon, S., M.R. Ammar, M. Erard, M. Amar, A.W. Moreau, P. Fossier, V. Gleize, N. Vitale, and N. Morel, 2013. *The V-ATPase membrane domain is a sensor of granular pH that controls the exocytotic machinery.* J Cell Biol, 203: 283-98.
84. Wang, D. and P.R. Hiesinger, 2013. *The vesicular ATPase: a missing link between acidification and exocytosis.* J Cell Biol, 203: 171-3.
85. Andenmatten, N., S. Egarter, A.J. Jackson, N. Jullien, J.P. Herman, and M. Meissner, 2012. *Conditional genome engineering in Toxoplasma gondii uncovers alternative invasion mechanisms.* Nat Methods, 10: 125-7.
86. Agop-Nersesian, C., B. Naissant, F. Ben Rached, M. Rauch, A. Kretzschmar, S. Thiberge, R. Menard, D.J. Ferguson, M. Meissner, and G. Langsley, 2009. *Rab11A-controlled assembly of the inner membrane complex is required for completion of apicomplexan cytokinesis.* PLoS Pathog, 5: e1000270.
87. Leung, J.M., J. Liu, L.A. Wetzel, and K. Hu, 2019. *Centrin2 from the human parasite Toxoplasma gondii is required for its invasion and intracellular replication.* J Cell Sci, 132.
88. Ebrahimzadeh, Z., A. Mukherjee, M.E. Crochetiere, A. Sergerie, S. Amiar, L.A. Thompson, D. Gagnon, D. Gaumond, R.V. Stahelin, J.B. Dacks, and D. Richard, 2019. *A pan-apicomplexan phosphoinositide-binding protein acts in malarial microneme exocytosis.* EMBO Rep, 20.
89. Nouvian, R., J. Neef, A.V. Bulankina, E. Reisinger, T. Pangrsic, T. Frank, S. Sikorra, N. Brose, T. Binz, and T. Moser, 2011. *Exocytosis at the hair cell ribbon synapse apparently operates without neuronal SNARE proteins.* Nat Neurosci, 14: 411-3.
90. Meriney, S.D., J.A. Umbach, and C.B. Gundersen, 2014. *Fast, Ca2+-dependent exocytosis at nerve terminals: shortcomings of SNARE-based models.* Prog Neurobiol, 121: 55-90.
91. Liu, Y., Y. Sugiura, T.C. Sudhof, and W. Lin, 2019. *Ablation of All Synaptobrevin vSNAREs Blocks Evoked But Not Spontaneous Neurotransmitter Release at Neuromuscular Synapses.* J Neurosci, 39: 6049-6066.

bioRxiv preprint doi: https://doi.org/10.1101/2020.04.27.063628; this version posted April 28, 2020. The copyright holder for this preprint (which was not certified by peer review) is the author/funder, who has granted bioRxiv a license to display the preprint in perpetuity. It is made available under aCC-BY-NC-ND 4.0 International license.

92. Lek, A., M. Lek, K.N. North, and S.T. Cooper, 2010. *Phylogenetic analysis of ferlin genes reveals ancient eukaryotic origins.* BMC Evol Biol, 10: 231.
93. Roos, D.S., R.G. Donald, N.S. Morrissette, and A.L. Moulton, 1994. *Molecular tools for genetic dissection of the protozoan parasite Toxoplasma gondii.* Methods Cell Biol, 45: 27-63.
94. Chen, C.T. and M.J. Gubbels, 2013. *The Toxoplasma gondii centrosome is the platform for internal daughter budding as revealed by a Nek1 kinase mutant.* J Cell Sci, 126: 3344-55.
95. Anderson-White, B.R., F.D. Ivey, K. Cheng, T. Szatanek, A. Lorestani, C.J. Beckers, D.J. Ferguson, N. Sahoo, and M.J. Gubbels, 2011. *A family of intermediate filament-like proteins is sequentially assembled into the cytoskeleton of Toxoplasma gondii.* Cell Microbiol, 13: 18-31.
96. Schaeffer, M., S.J. Han, T. Chtanova, G.G. van Dooren, P. Herzmark, Y. Chen, B. Roysam, B. Striepen, and E.A. Robey, 2009. *Dynamic imaging of T cell-parasite interactions in the brains of mice chronically infected with Toxoplasma gondii.* J Immunol, 182: 6379-93.
97. Alexandrov, A., M. Vignali, D.J. LaCount, E. Quartley, C. de Vries, D. De Rosa, J. Babulski, S.F. Mitchell, L.W. Schoenfeld, S. Fields, W.G. Hol, M.E. Dumont, E.M. Phizicky, and E.J. Grayhack, 2004. *A facile method for high-throughput co-expression of protein pairs.* Mol Cell Proteomics, 3: 934-8.
98. Gubbels, M.J., S. Vaishnava, N. Boot, J.F. Dubremetz, and B. Striepen, 2006. *A MORN-repeat protein is a dynamic component of the Toxoplasma gondii cell division apparatus.* J Cell Sci, 119: 2236-45.
99. Abramoff, M.D., P.J. Magalhaes, and S.J. Ram, 2004. *Image Processing with ImageJ.* Biophotonics International, 11: 36-42.
100. Schindelin, J., I. Arganda-Carreras, E. Frise, V. Kaynig, M. Longair, T. Pietzsch, S. Preibisch, C. Rueden, S. Saalfeld, B. Schmid, J.Y. Tinevez, D.J. White, V. Hartenstein, K. Eliceiri, P. Tomancak, and A. Cardona, 2012. *Fiji: an open-source platform for biological-image analysis.* Nat Methods, 9: 676-82.
101. Coppens, I. and K.A. Joiner, 2003. *Host but not parasite cholesterol controls Toxoplasma cell entry by modulating organelle discharge.* Mol Biol Cell, 14: 3804-20.
102. Carey, K.L., N.J. Westwood, T.J. Mitchison, and G.E. Ward, 2004. *A small-molecule approach to studying invasive mechanisms of Toxoplasma gondii.* Proc Natl Acad Sci U S A, 101: 7433-8.
103. Carruthers, V.B. and L.D. Sibley, 1999. *Mobilization of intracellular calcium stimulates microneme discharge in Toxoplasma gondii.* Mol Microbiol, 31: 421-8.
104. Jimenez, J.L. and R. Bashir, 2007. *In silico functional and structural characterisation of ferlin proteins by mapping disease-causing mutations and evolutionary information onto three-dimensional models of their C2 domains.* J Neurol Sci, 260: 114-23.
105. Hartmann, J., K. Hu, C.Y. He, L. Pelletier, D.S. Roos, and G. Warren, 2006. *Golgi and centrosome cycles in Toxoplasma gondii.* Mol Biochem Parasitol, 145: 125-7.
106. Wan, K.L., V.B. Carruthers, L.D. Sibley, and J.W. Ajioka, 1997. *Molecular characterisation of an expressed sequence tag locus of Toxoplasma gondii encoding the micronemal protein MIC2.* Mol Biochem Parasitol, 84: 203-14.
107. Garcia-Reguet, N., M. Lebrun, M.N. Fourmaux, O. Mercereau-Puijalon, T. Mann, C.J. Beckers, B. Samyn, J. Van Beeumen, D. Bout, and J.F. Dubremetz, 2000. *The microneme*

bioRxiv preprint doi: https://doi.org/10.1101/2020.04.27.063628; this version posted April 28, 2020. The copyright holder for this preprint (which was not certified by peer review) is the author/funder, who has granted bioRxiv a license to display the preprint in perpetuity. It is made available under aCC-BY-NC-ND 4.0 International license.

protein MIC3 of Toxoplasma gondii is a secretory adhesin that binds to both the surface of the host cells and the surface of the parasite. Cell Microbiol, 2: 353-64.

108. Brydges, S.D., X.W. Zhou, M.H. Huynh, J.M. Harper, J. Mital, K.D. Adjogble, W. Daubener, G.E. Ward, and V.B. Carruthers, 2006. *Targeted deletion of MIC5 enhances trimming proteolysis of Toxoplasma invasion proteins.* Eukaryot Cell, 5: 2174-83.

109. Meissner, M., M. Reiss, N. Viebig, V.B. Carruthers, C. Toursel, S. Tomavo, J.W. Ajioka, and D. Soldati, 2002. *A family of transmembrane microneme proteins of Toxoplasma gondii contain EGF-like domains and function as escorters.* J Cell Sci, 115: 563-74.

110. Hoff, E.F., S.H. Cook, G.D. Sherman, J.M. Harper, D.J. Ferguson, J.F. Dubremetz, and V.B. Carruthers, 2001. *Toxoplasma gondii: molecular cloning and characterization of a novel 18-kDa secretory antigen, TgMIC10.* Exp Parasitol, 97: 77-88.

111. Harper, J.M., M.H. Huynh, I. Coppens, F. Parussini, S. Moreno, and V.B. Carruthers, 2006. *A cleavable propeptide influences Toxoplasma infection by facilitating the trafficking and secretion of the TgMIC2-M2AP invasion complex.* Molecular Biology of the Cell, 17: 4551-4563.

112. Carey, K.L., A.M. Jongco, K. Kim, and G.E. Ward, 2004. *The Toxoplasma gondii rhoptry protein ROP4 is secreted into the parasitophorous vacuole and becomes phosphorylated in infected cells.* Eukaryot Cell, 3: 1320-30.

113. Cesbron-Delauw, M.F., B. Guy, G. Torpier, R.J. Pierce, G. Lenzen, J.Y. Cesbron, H. Charif, P. Lepage, F. Darcy, and J.P. Lecocq, 1989. *Molecular characterization of a 23-kilodalton major antigen secreted by Toxoplasma gondii.* Proc Natl Acad Sci U S A, 86: 7537-41.

114. Burg, J.L., D. Perelman, L.H. Kasper, P.L. Ware, and J.C. Boothroyd, 1988. *Molecular analysis of the gene encoding the major surface antigen of Toxoplasma gondii.* Journal of immunology, 141: 3584-91.

115. Dubremetz, J.F., A. Achbarou, D. Bermudes, and K.A. Joiner, 1993. *Kinetics and pattern of organelle exocytosis during Toxoplasma gondii/host-cell interaction.* Parasitol Res, 79: 402-8.

116. Couvreur, G., A. Sadak, B. Fortier, and J.F. Dubremetz, 1988. *Surface antigens of Toxoplasma gondii.* Parasitology, 97 (Pt 1): 1-10.

117. Sadak, A., Z. Taghy, B. Fortier, and J.F. Dubremetz, 1988. *Characterization of a Family of Rhoptry Proteins of Toxoplasma-Gondii.* Molecular and Biochemical Parasitology, 29: 203-211.

118. Morrissette, N.S. and L.D. Sibley, 2002. *Disruption of microtubules uncouples budding and nuclear division in Toxoplasma gondii.* J Cell Sci, 115: 1017-25.

119. Jerka-Dziadosz, M., L.M. Jenkins, E.M. Nelsen, N.E. Williams, R. Jaeckel-Williams, and J. Frankel, 1995. *Cellular polarity in ciliates: persistence of global polarity in a disorganized mutant of Tetrahymena thermophila that disrupts cytoskeletal organization.* Dev Biol, 169: 644-61.

bioRxiv preprint doi: https://doi.org/10.1101/2020.04.27.063628; this version posted April 28, 2020. The copyright holder for this preprint (which was not certified by peer review) is the author/funder, who has granted bioRxiv a license to display the preprint in perpetuity. It is made available under aCC-BY-NC-ND 4.0 International license.

Figure 1

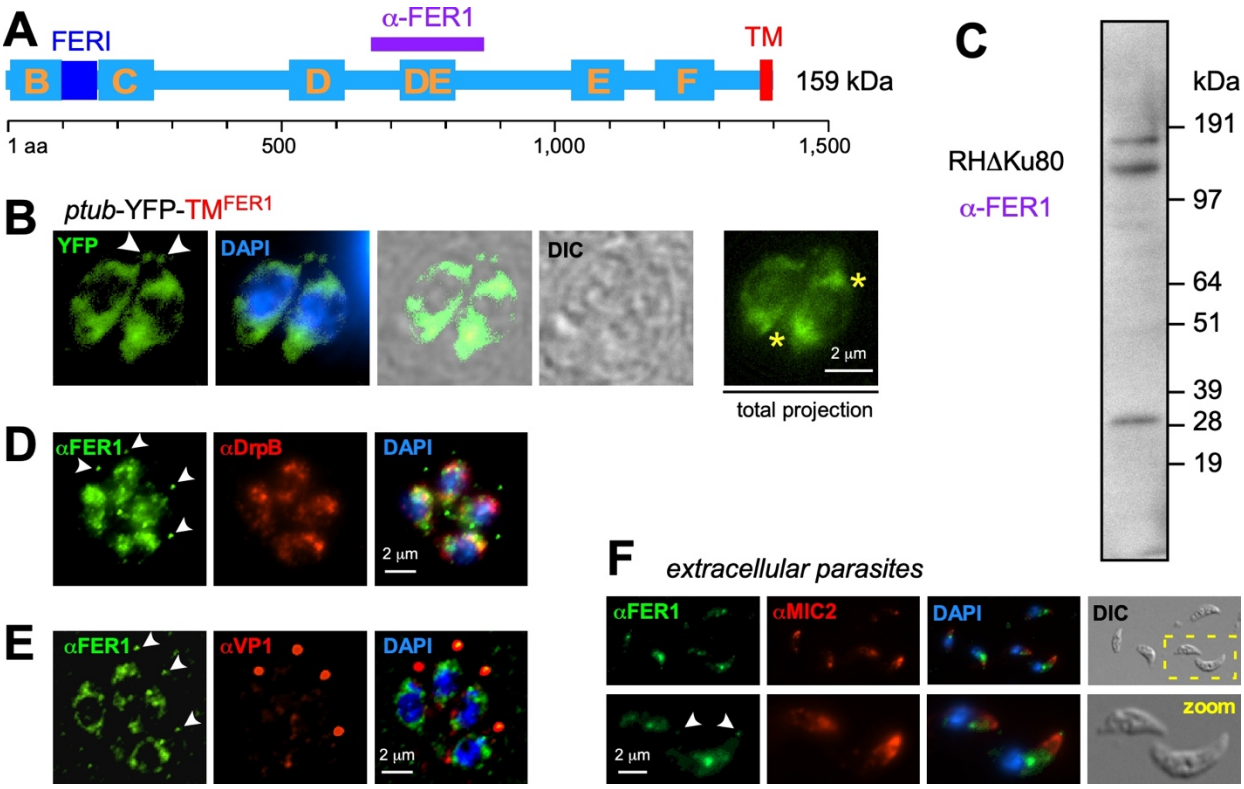

Figure 1. FER1 localizes to the secretory pathway and the conoid region. A. Schematic representation of TgFER1. Yellow letters mark the C2 domains; the aa 669-877 region used to generate a specific antiserum is marked in purple; FERI is a domain conserved in most ferlins with unknown function; TM is the transmembrane domain. **B.** Overexpression of a YFP fusion to the FER1 TM domain (C-terminal 31 aa, comprising 10 aa before the 21 extremely C-terminal TM domain) only under the tubulin promoter (*ptub*). Arrowheads mark YFP localization to the conoid region; yellow asterisk mark the perinuclear region reminiscent of the ER. Left panels represent a single z-layer from deconvolved images collected by wide-field microscopy; in the right panel all z-stacks are projected. **C.** Western blot analysis with the affinity purified guinea pig polyclonal antiserum generated against the FER1 region marked in panel A. Total lysate of wild type (RHΔKu80) parasites was loaded. **D-F.** Analysis of the affinity purified FER1 antiserum by IFA co-stained with α-DrpB serum marking the ELC (D) and α-VP1 serum marking the plant like vacuole (E). Arrowheads mark FER1 localization to the conoid region, which colocalizes with VP1. The area corresponding with the yellow box in the top right panel of F is magnified in the lower panels (zoom). Parasites in A and F were fixed with 4% PFA, parasites in D and E with 100% methanol.

bioRxiv preprint doi: https://doi.org/10.1101/2020.04.27.063628; this version posted April 28, 2020. The copyright holder for this preprint (which was not certified by peer review) is the author/funder, who has granted bioRxiv a license to display the preprint in perpetuity. It is made available under aCC-BY-NC-ND 4.0 International license.

Figure 2

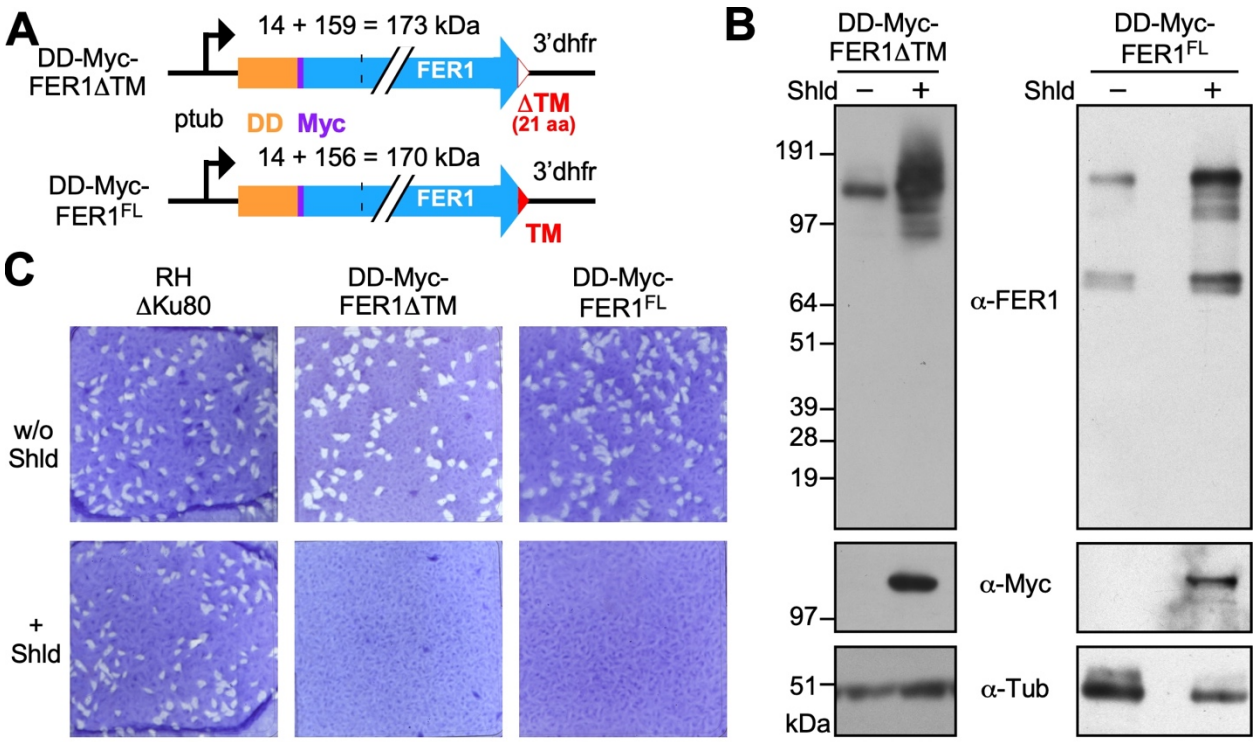

Figure 2. Generation and validation of conditional FER1 overexpression parasite lines. A. Schematic representation of the overexpression constructs driven by the strong constitutive α-tubulin promoter (*ptub*). DD: destabilization domain; Myc: cMyc epitope tag; TM: transmembrane domain; FL: full length. **B.** Western blot analysis of the overexpression parasite lines. Polyclonal guinea pig FER1 antiserum as in Fig 1. Monoclonal antibody12G10 recognizing α-tubulin was used as loading control. Parasites were induced with 1 µM Shield-1 for 24 hrs. **C.** plaque assays of infected HFF monolayers grown for 7 days ± 1 µM Shield-1.

bioRxiv preprint doi: https://doi.org/10.1101/2020.04.27.063628; this version posted April 28, 2020. The copyright holder for this preprint (which was not certified by peer review) is the author/funder, who has granted bioRxiv a license to display the preprint in perpetuity. It is made available under aCC-BY-NC-ND 4.0 International license.

1176 **Figure 3**

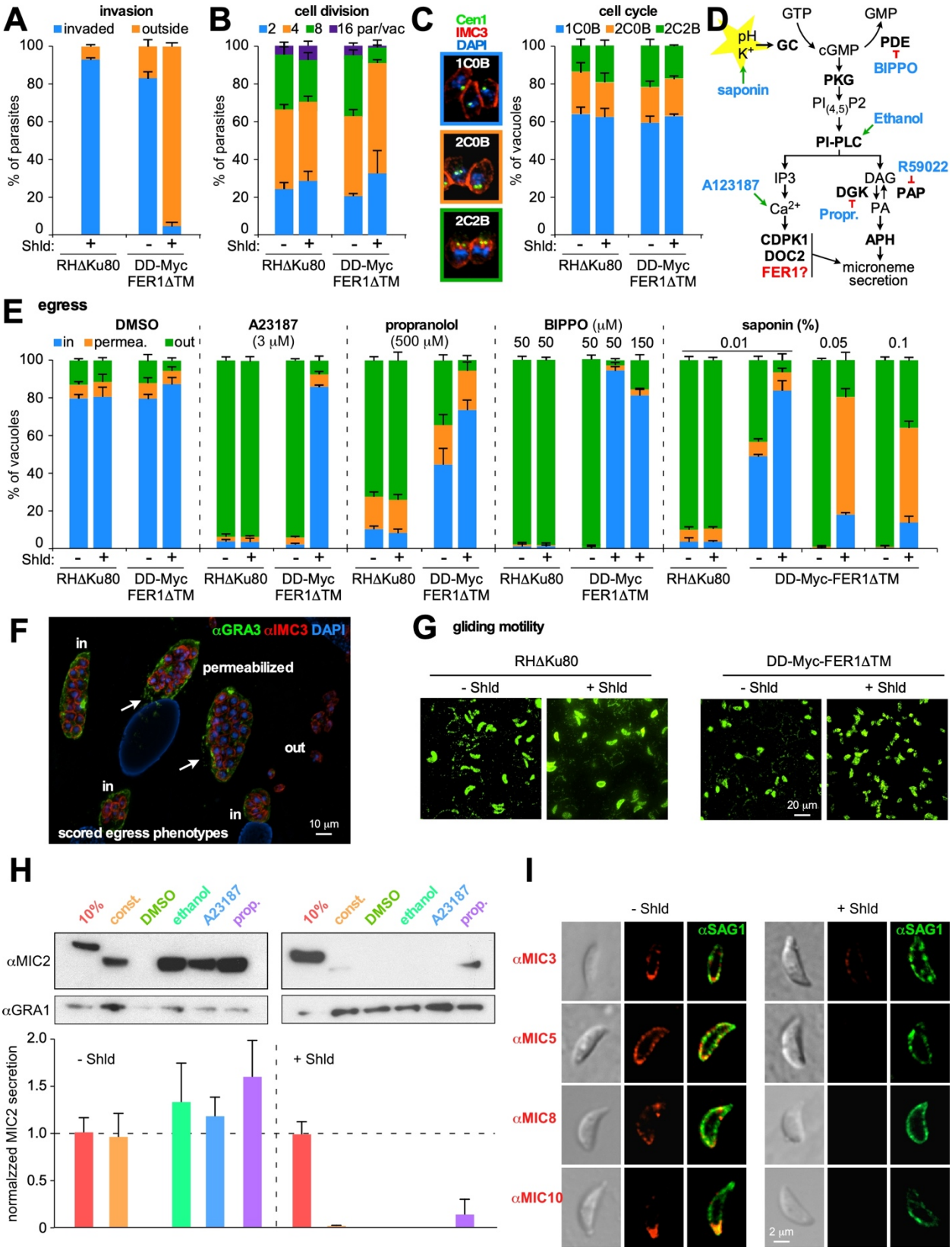

1177

bioRxiv preprint doi: https://doi.org/10.1101/2020.04.27.063628; this version posted April 28, 2020. The copyright holder for this preprint (which was not certified by peer review) is the author/funder, who has granted bioRxiv a license to display the preprint in perpetuity. It is made available under aCC-BY-NC-ND 4.0 International license.

Figure 3. Phenotypic characterization of parasites overexpressing DD-Myc-FER1ΔTM. A. Red-green invasion assay data reveal an invasion defect. **B, C.** Cell division and cell cycle progression analysis show that overexpression of DD-Myc-FER1ΔTM results in slightly slower reproduction rates (B), however a significant delay in cell cycle was not detected (C). Examples of the cell cycle stages quantified in the left of panel C are shown on the right. Parasites were allowed to invade for 2 hrs upon which 1 µM Shield-1 was added for 18 hrs. p=0.031 (*t*-test) accumulation of parasite in the 4-cells/vacuole stage. **D.** Schematic overview of signaling toward microneme secretion and egress, highlighting pharmacological agents acting on various events. **E, F.** Induced egress assays. Parasites grown for 30 hrs in fibroblasts and induced for 18 hrs with 1 µM Shield-1 were triggered for egress with the pharmacologicals as indicated, fixed and stained with α-IMC3 (parasite cortex) and α-GRA3 (PVM) sera and scored for status of vacuole permeabilization and/or egress (F; representative image; arrows mark holes in the PVM of permeabilized vacuoles). n=3±std. Parasites were not under Shield-1 pressure during the 5 min pharmacological incubation. **G.** Trail assay using α-SAG1 serum to assess gliding motility capacity reveals that DD-Myc-FER1ΔTM parasites are unable to glide. Parasites were induced for 18 hrs ± 1 µM Shield-1, mechanically released from host cells and kept under 1 µM Shield-1 throughout the 30 min gliding experiment at 37ºC. **H.** Assessment of microneme secretion by western blot detection of MIC2 released in the supernatant under various triggers. Parasites were induced 18 hrs with 1 µM Shield-1 and harvested by physical release from the host cell. 10%: 10% of total lysate; const.: 1 hr constitutive secretion at 37ºC in absence of secretagogue; 1% ethanol; 2 µM A23187; 500 µM propranolol. DMSO is the vehicle control for A23187. Induced secretion for 5 min at 37ºC. Bottom of panel represents quantified secretion normalized to the GRA1 signal and to the 10% loading control for each condition. n=3±std. Parent line controls in Supplementary Fig S1. Parasites were not under Shield-1 pressure during secretion assay. **I.** Secretion of the Rab5/A-dependent microneme population was assessed by IFA on non-permeabilized parasites induced for 18 hrs ± 1 µM Shield-1, mechanically released, and exposed to fresh host cells for 5 min at 37ºC. Parasites were not under Shield-1 pressure during assay.

bioRxiv preprint doi: https://doi.org/10.1101/2020.04.27.063628; this version posted April 28, 2020. The copyright holder for this preprint (which was not certified by peer review) is the author/funder, who has granted bioRxiv a license to display the preprint in perpetuity. It is made available under aCC-BY-NC-ND 4.0 International license.

Figure 4

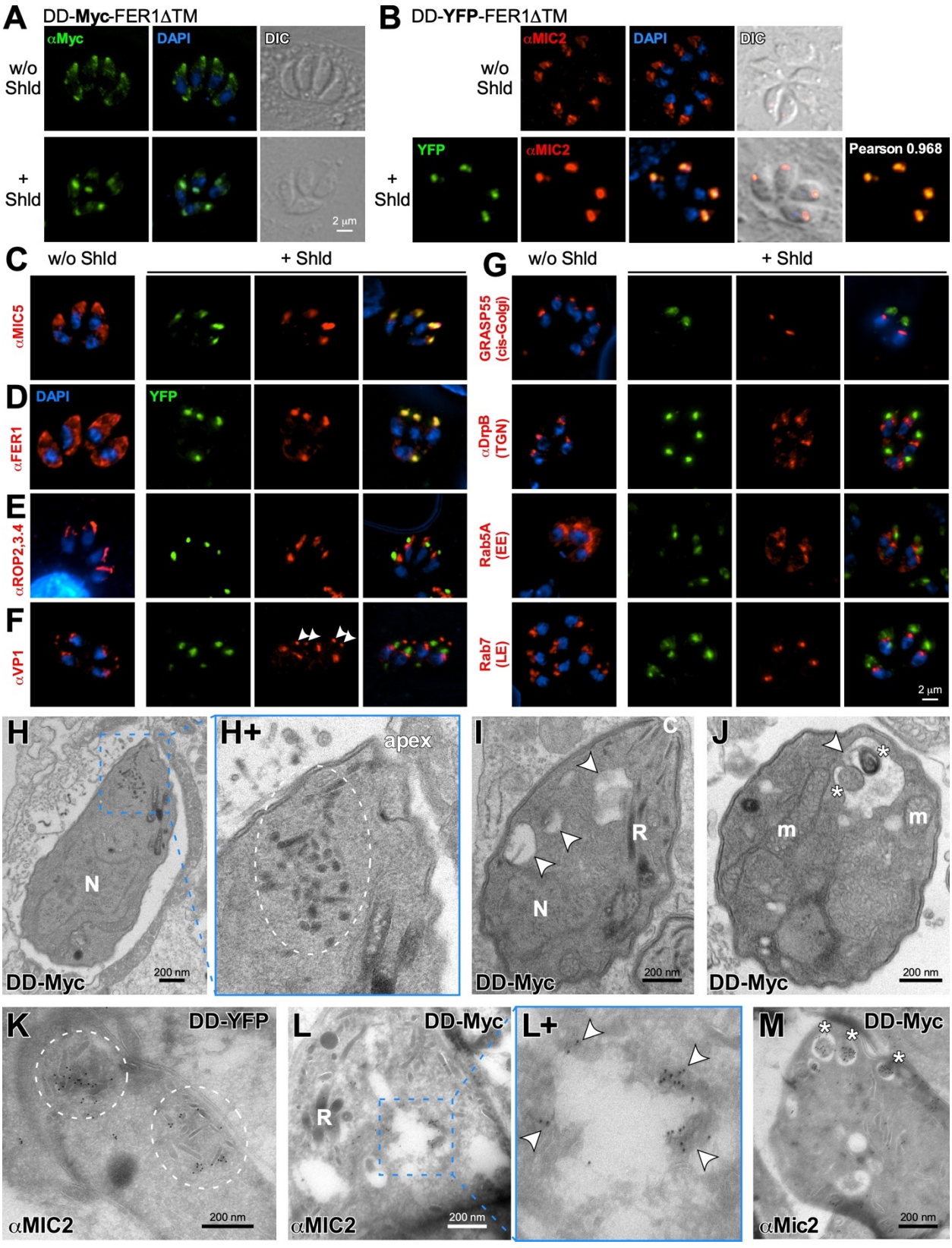

bioRxiv preprint doi: https://doi.org/10.1101/2020.04.27.063628; this version posted April 28, 2020. The copyright holder for this preprint (which was not certified by peer review) is the author/funder, who has granted bioRxiv a license to display the preprint in perpetuity. It is made available under aCC-BY-NC-ND 4.0 International license.

Fig 4. Overexpression of dominant negative FER1ΔTM constructs result in microneme mislocalization. A, B. Overexpression of DD-**Myc**-FER1ΔTM (A) or DD-**YFP**-FER1ΔTM (B) leads to accumulation of microneme protein, visualized with α-MIC2, in a central, apical location. YFP and MIC2 co-localization was assesses by Pearson correlation. **C.** Microneme proteins of the Rab5A/C-dependent trafficking pathway, visualized with α-MIC5, also accumulate in the FER1 compartment. **D.** α-FER1 serum confirms exclusive accumulation in the microneme protein compartment. **E.** ROP proteins do not accumulate and rhoptry morphology is normal. **F.** Co-localization of VP1 and the YFP accumulation is not detected. Note the apical VP1 localization is still present (arrowheads). **G.** Markers for cis Golgi, trans-Golgi network (TGN) as well as early (EE) and late (LE) endosome markers localize normally and do no co-localize with the YFP accumulation. In all IFA experiments parasites were treated with 1 µM Shield-1 for 18 hrs; results with additional independent markers for the same compartments are provided in Supplementary Fig S2. **H-J.** TEM of DD-Myc-FER1ΔTM overexpressing parasites induced for 16 hrs with 1 µM Shield-1. N, nucleus; R, rhoptries; m, mitochondrion. Dotted circle marks atypical accumulation of microneme organelles in the apical end. Arrowheads mark enlarged vacuoles, sometimes with *-marked accumulations inside. **K-M.** IEM with MIC2 antibody (10 nm gold particles) of DD-Myc-FER1ΔTM or of DD-YFP-FER1ΔTM overexpressing parasites induced for either 7 hrs with 3 µM Shield-1 (K,M) or 16 hrs with 1 µM Shield-1 (L). Dotted circles mark atypical microneme accumulations in the cytosol. R, rhoptries. Arrowheads mark MIC2 signal at the edge of an enlarged vacuole. Asterisks mark accumulations inside vacuoles containing MIC2 protein.

bioRxiv preprint doi: https://doi.org/10.1101/2020.04.27.063628; this version posted April 28, 2020. The copyright holder for this preprint (which was not certified by peer review) is the author/funder, who has granted bioRxiv a license to display the preprint in perpetuity. It is made available under aCC-BY-NC-ND 4.0 International license.

1229 **Figure 5**

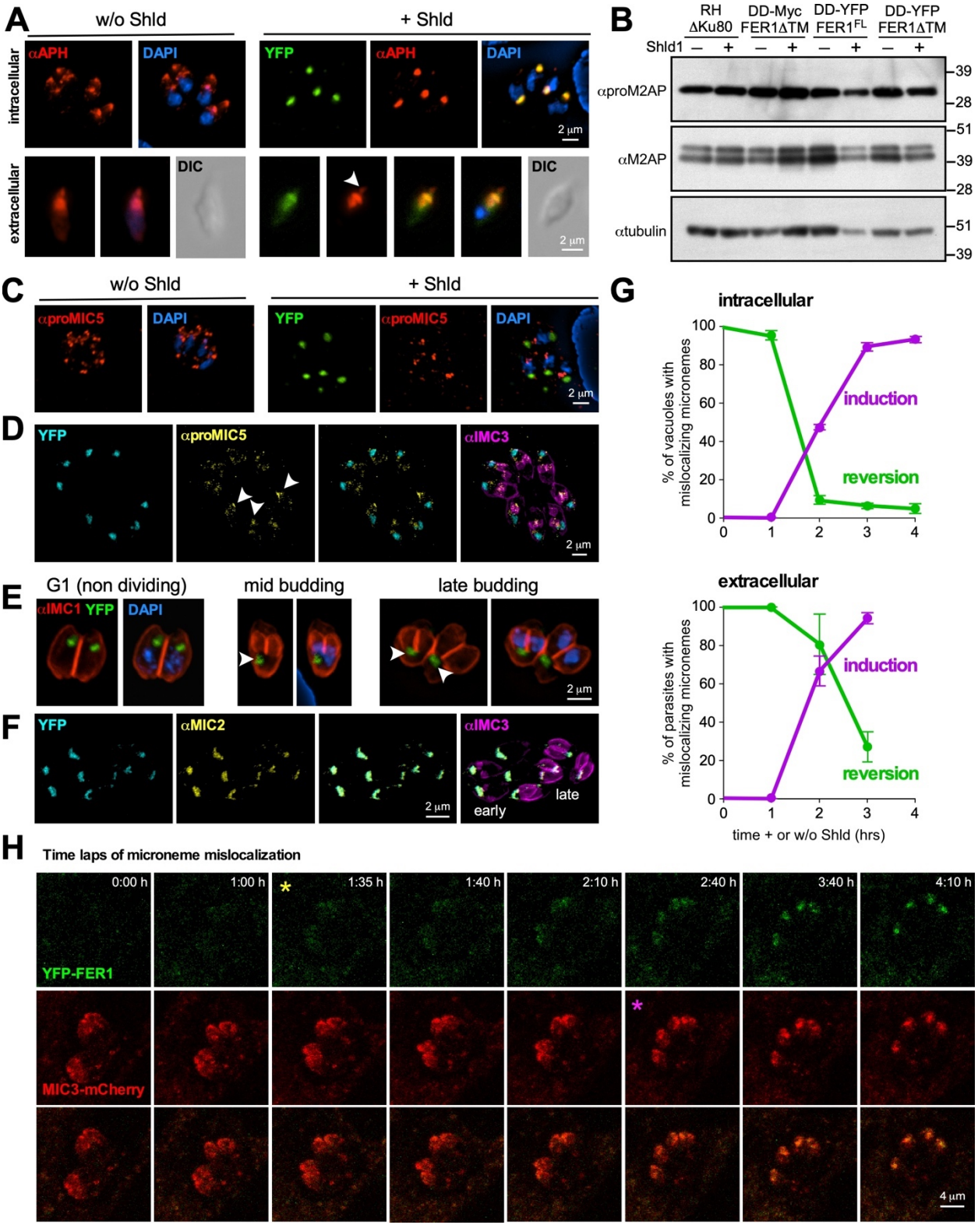

1230

1231

bioRxiv preprint doi: https://doi.org/10.1101/2020.04.27.063628; this version posted April 28, 2020. The copyright holder for this preprint (which was not certified by peer review) is the author/funder, who has granted bioRxiv a license to display the preprint in perpetuity. It is made available under aCC-BY-NC-ND 4.0 International license.

Figure 5. Microneme trafficking dynamics upon DD-YFP-FER1ΔTM overexpression. In all IFA experiments parasites were treated with 1 µM Shield-1 for 18 hrs. **A.** Mislocalized micronemes are coated with the mature microneme marker APH in both intracellular (top) and extracellular (bottom) parasites. Arrowhead marks APH signal in the conoid where YFP signal is absent. **B.** Normal maturation by pro-peptide processing in the ELC-PLV compartment of microneme proteins in induced and various control parasites as indicated was demonstrated by western blot using antiserum against the pro-peptide of M2AP (α-proM2AP) and antiserum against the mature section of the protein (α-M2AP). α-tubulin serves as loading control. **C.** IFA with α-proMIC5 revealed that microneme accumulation is not due to arrested trafficking since proMIC5 is only observed in the ELC-PLV compartment in newly forming daughter buds. **D.** Induced mutants co-stained with YFP, proMIC5, and IMC3 antiserum to track the timing and localization of proMIC5 processed as indicated. Arrowheads mark the proMIC5 compartment within budding daughter buds. Note that DD-YFP-FER1ΔTM is exclusively present in the mother parasites and does not localize to the budding daughters**. E.** Induced mutants co-stained with IMC1 antiserum to track division stages as indicated. Arrowheads mark the mother parasite's YFP accumulation migrating into a basal direction during progression of daughter budding. Note the absence of YFP in the daughter buds.
F. Induced mutants co-stained with YFP, MIC2, and IMC3 antisera to track the localization of mature MIC2 protein through cell division. Note the consistent colocalization of DD-YFP-FER1ΔTM with MIC2 throughout the division stages, indicating that the daughter buds never assemble mature micronemes. **G.** Time courses of the incidence of vacuoles or individual parasites with mislocalizing micronemes in intracellular and extracellular parasites, respectively, visualized through α-MIC2 IFA. At least 100 vacuoles or parasites were counted per time point. n=3±std. In reversion experiments, intracellular parasites were induced for 18 hrs with Shield-1.
H. Select panels from time lapse experiment with DD-YFP-FER1ΔTM parasites co-transfected with MIC3-mCherry to track microneme localization dynamics. At t=0, 2 µM Shield-1 was added. The first time point at which the piling up of YFP-FER1 could be convincingly observed is marked with a yellow asterisk; the first time where MIC3-mCherry can be seen re-localizing from the apical cortex to the central apical localization co-localizing with YFP-FER1 is marked with a purple asterisk. Panels from supplementary movie S1.

bioRxiv preprint doi: https://doi.org/10.1101/2020.04.27.063628; this version posted April 28, 2020. The copyright holder for this preprint (which was not certified by peer review) is the author/funder, who has granted bioRxiv a license to display the preprint in perpetuity. It is made available under aCC-BY-NC-ND 4.0 International license.

1262 **Figure 6**

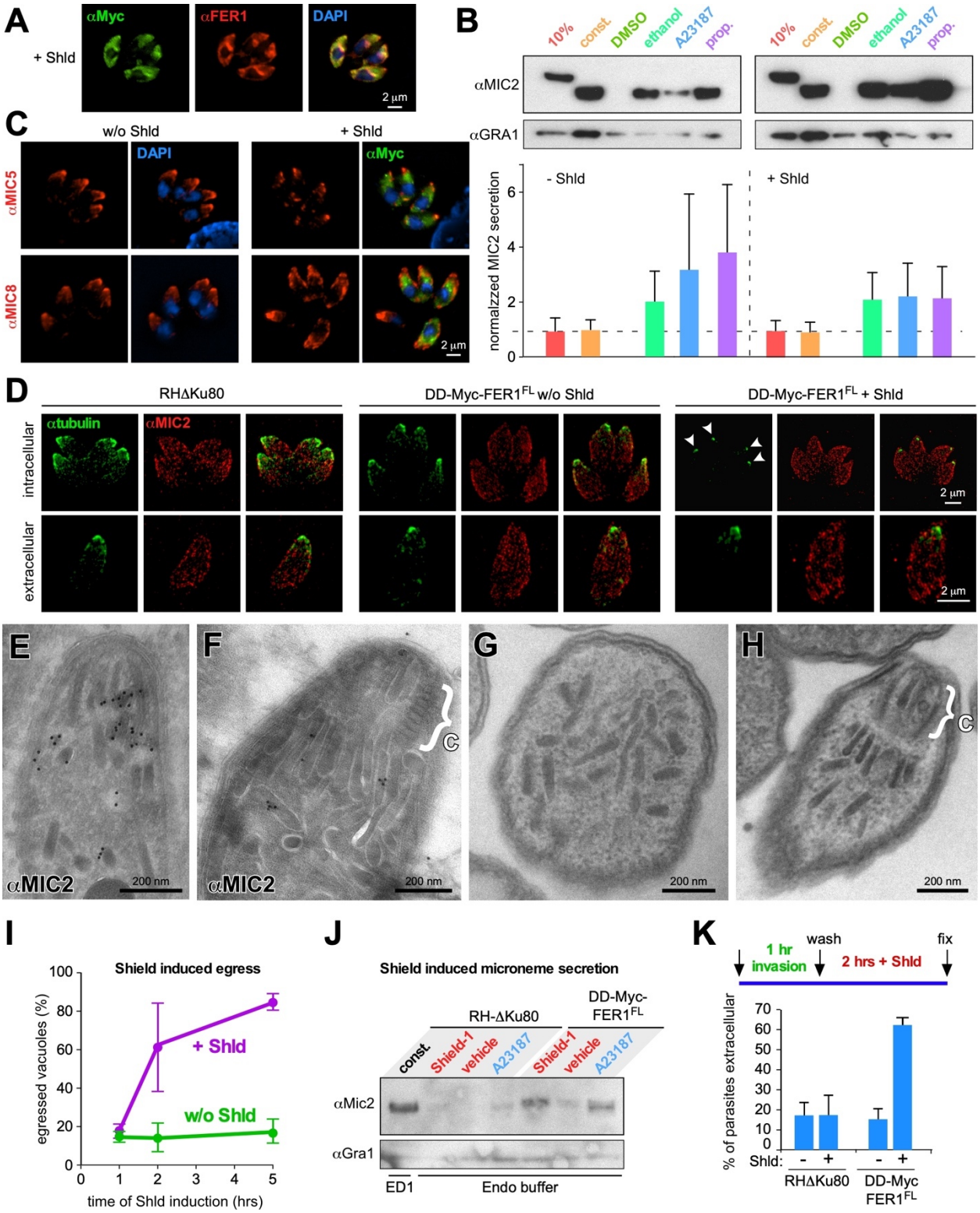

1263

1264

1265

bioRxiv preprint doi: https://doi.org/10.1101/2020.04.27.063628; this version posted April 28, 2020. The copyright holder for this preprint (which was not certified by peer review) is the author/funder, who has granted bioRxiv a license to display the preprint in perpetuity. It is made available under aCC-BY-NC-ND 4.0 International license.

Figure 6. DD-Myc-FER1^{FL} overexpression results in apical microneme migration and a burst of signaling-independent microneme release. A. Co-staining of α-Myc and α-FER1 sera by IFA shows that overexpressed DD-Myc-FER1^{FL} localizes to the cytoplasm. Total projection of deconvolved image is shown. **B.** Assessment of microneme secretion by western blot through MIC2 release in the supernatant under various triggers. Parasites were induced 6 hrs with 1 µM Shield-1 and harvested by physical release from the host cell. 10%: 10% of total lysate; const.: 1 hr constitutive secretion at 37ºC in absence of secretagogue; 1% ethanol; 2 µM A23187; 500 µM propranolol. DMSO is the vehicle control for A23187. Induced secretion for 5 min at 37ºC. Bottom of panel represents quantified secretion normalized to the GRA1 signal and to the 10% loading control for each condition. n=3±std. Parent line controls in Supplementary Fig S1. **C.** Immunofluorescence of DD-Myc-FER1^{FL} co-stained with α-MIC5 and α-MIC8 and α-FER1 shows that this Rab5A/C-dependent microneme population becomes scattered upon phenotype induction, although an extreme apical focal point remains. **D.** Super-resolution SIM microscopy of wild-type and DD-Myc-FER1^{FL} co-stained with α-MIC2 and α-Tgβ-tubulin further details apical microneme translocation in intracellular parasites upon Shield-1 induction (arrowheads). In extracellular parasites an increased apical accumulation of micronemes is seen across control and mutant parasites regardless of phenotype induction. **E, F.** IEM of DD-Myc-FER1^{FL} overexpressing parasites stained with MIC2 antibody (10 nm gold particles) induced for 16 hrs with 1 µM Shield-1. MIC signal localizes to apically accumulated micronemes which display a stretched or extended morphology. Accolade bracket marks conoid (c). **G, H.** TEM of extracellular DD-Myc-FER1^{FL} overexpressing parasites induced for 3 hrs with 2 µM Shield-1. Cross section in J shows the extended feature or the densely packed microneme organelles, whereas K shows the radial micronemes just below the conoid, again with a slightly stretched or extended appearance. Accolade bracket marks conoid (c). **I.** Time course of Shield-1 Induced egress. Parasites grown for 30 hrs in fibroblasts and induced for 1 µM Shield-1 for the times as indicated, fixed with 100% methanol and stained with α-Myc, α-MIC8 and DAPI. Intact vacuoles per field were scored as proxy for egress. n=3±std. **J.** Shield-1 induced microneme secretion in Endo buffer. Western blot of MIC2 release in the supernatant; GRA1 as control. Const.: Constitutive 1 hr at 37ºC in standard ED1 culture medium. In intracellular conditions mimicking Endo buffer, parasites were induced with 1 µM Shield-1 for 2 hrs at 37ºC; vehicle represent the solvent of the Shield-1 stock (0.1% ethanol end concentration). A23187 (1 µM)

bioRxiv preprint doi: https://doi.org/10.1101/2020.04.27.063628; this version posted April 28, 2020. The copyright holder for this preprint (which was not certified by peer review) is the author/funder, who has granted bioRxiv a license to display the preprint in perpetuity. It is made available under aCC-BY-NC-ND 4.0 International license.

was added for 5 min in the end of the 2 hr window and is additive to the constitutive secretion. **K.** Modified red-green invasion assay followed by Shield-1 induction. Top schematic shows parasites were allowed to invade for 1 hr min at 37ºC followed by a wash to remove non-invaded parasites and 2 hrs 1 μM Shield-1 induction followed by the red-green invasion assay. Lower panel shows the relative number of parasites observed outside the host cell, indicating overexpression of FER1 leads to microneme secretion, egress, and host cell destruction. n=4±std.

bioRxiv preprint doi: https://doi.org/10.1101/2020.04.27.063628; this version posted April 28, 2020. The copyright holder for this preprint (which was not certified by peer review) is the author/funder, who has granted bioRxiv a license to display the preprint in perpetuity. It is made available under aCC-BY-NC-ND 4.0 International license.

Figure 7 - FER1 is Ca^{2+}dependendent

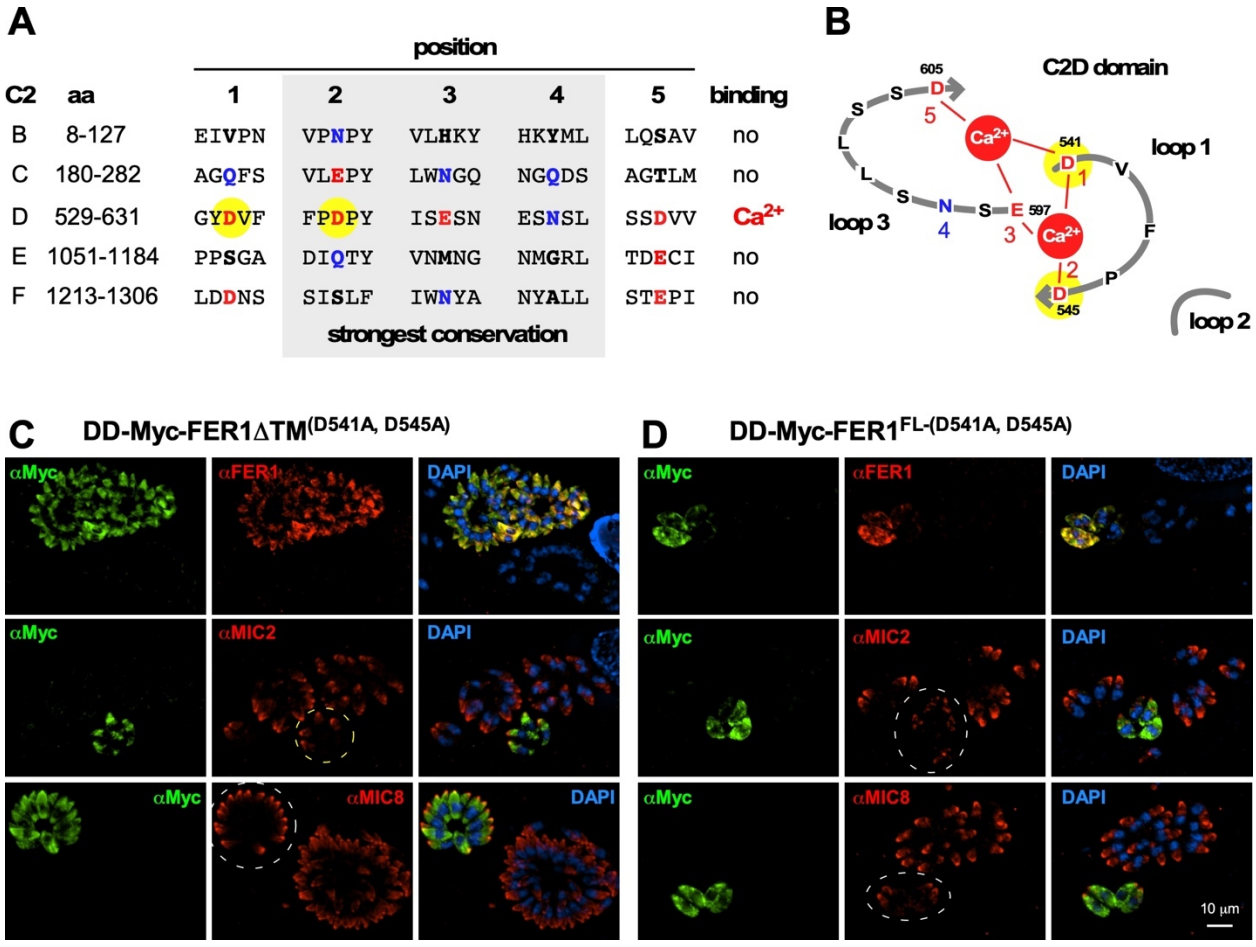

Figure 7. FER1-mediated trafficking of micronemes relies on predicted Ca^{2+}-binding residues. A. Sequence analysis of the five conserved key positions (#1-5) in the C2A-F domain loops interfacing with Ca^{2+} [104]. D or E residues (red) stabilize Ca^{2+}, N or Q (bleu) are expected to support phospholipid binding. Positions 2, 3, and 4 shaded in grey are more strongly conserved than positions 1 and 5. Yellow highlighted residues were mutated to A to abolish the predicted Ca^{2+}-binding capacity in the C2D domain resulting in the mutant $FER1^{(DD541,545AA)}$ allele. **B.** Models of the C2D domain loops and putative Ca^{2+} binding capacity. Yellow highlighted residues as in panel A. **C, D.** Transient overexpression DD-Myc-$FER1\Delta TM^{(D541A,D545A)}$ DD-Myc-$FER1^{FL-(D541A,D545A)}$, respectively, co-stained for Myc, FER1, MIC2 and MIC8, as indicated. Each panel contains transfected (Myc positive) and non-transfected (Myc negative) parasite examples. Note that due to the high level of overexpression

bioRxiv preprint doi: https://doi.org/10.1101/2020.04.27.063628; this version posted April 28, 2020. The copyright holder for this preprint (which was not certified by peer review) is the author/funder, who has granted bioRxiv a license to display the preprint in perpetuity. It is made available under aCC-BY-NC-ND 4.0 International license.

1318 the FER1 signal in non-transfected parasites is below the detection limit under these conditions.
1319 Following electroporation, parasites were allowed to invade for 2 hrs before 1 μM Shield-1
1320 induction for 24 hrs. Yellow dotted circle marks normal MIC morphology while white dotted
1321 circles mark aberrant MIC morphology in vacuoles overexpressing the D541A,545A FER1
1322 alleles as indicated.

bioRxiv preprint doi: https://doi.org/10.1101/2020.04.27.063628; this version posted April 28, 2020. The copyright holder for this preprint (which was not certified by peer review) is the author/funder, who has granted bioRxiv a license to display the preprint in perpetuity. It is made available under aCC-BY-NC-ND 4.0 International license.

Figure 8

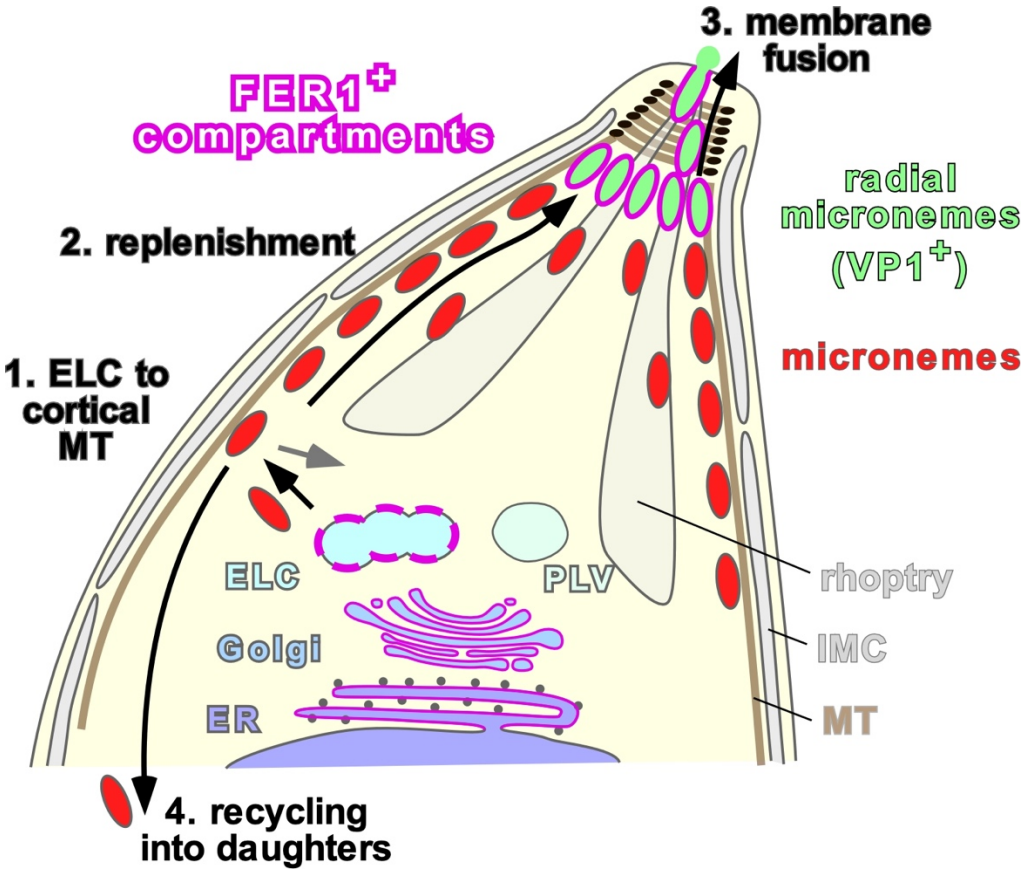

Figure 8. Working model of FER1 mediated microneme events. FER1 mediates the following trafficking steps: 1. From the ELC to the subpellicular microtubules (actin dependent); 2. microneme migration along the subpellicular microtubules; 3. Microneme membrane fusion with the plasma membrane; 4. Recycling of micronemes into the budding daughters (actin dependent). We hypothesize the radial micronemes represent a readily releasable vesicle pool primed for secretion by VP1-mediated acidification. MT: microtubules; ELC: endosome-like compartment; PLV: plant like vacuole or VAC.

bioRxiv preprint doi: https://doi.org/10.1101/2020.04.27.063628; this version posted April 28, 2020. The copyright holder for this preprint (which was not certified by peer review) is the author/funder, who has granted bioRxiv a license to display the preprint in perpetuity. It is made available under aCC-BY-NC-ND 4.0 International license.

Supplementary data

Supplementary Movie S1. Time lapse experiment of DD-YFP-FER1ΔTM parasites co-transfected with MIC3-mCherry to track the micronemes. At t=0, 2 µM Shield-1 was added and images collected every 5 minutes. Scale bars 80 µm.

Supplementary movie S2. Time lapse experiment of DD-YFP-FER1ΔTM parasites co-transfected with IMC3-mCherry to track cell division status. At t=0, 2 µM Shield-1 was added and images collected every 5 minutes. Scale bars 80 µm.

Supplementary Figure S1

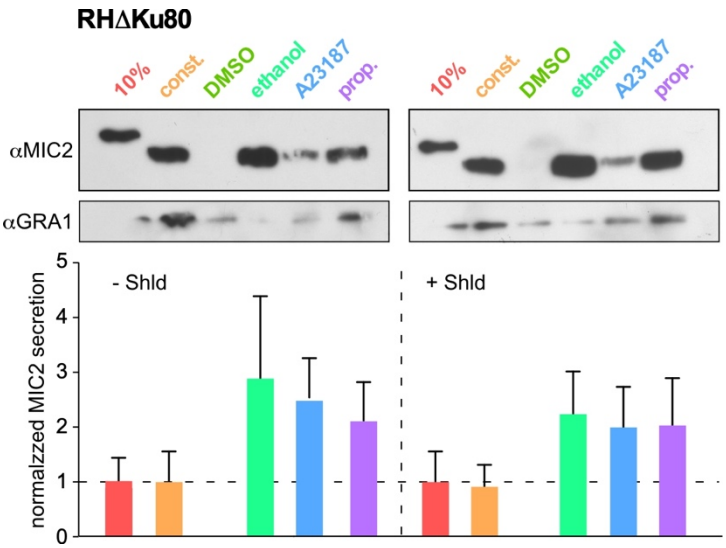

Supplementary Figure S1. Microneme secretion assessment of the RHΔKu80 parent line control. Assessment of microneme secretion by western blotting by detecting MIC2 release in the supernatant under various triggers. Parasites were induced 18 hrs with 1 µM Shield-1 and harvested by physical release from the host cell. 10%: 10% of total lysate; const.: 1 hr constitutive secretion at 37ºC in absence of secretagogue; 1% ethanol; 2 µM A23187; 500 µM propranolol. DMSO is the vehicle control for A23187. Induced secretion for 5 min at 37ºC. Bottom of panel represents quantified secretion normalized to the GRA1 signal and to the 10% loading control for each condition. n=3±std.

bioRxiv preprint doi: https://doi.org/10.1101/2020.04.27.063628; this version posted April 28, 2020. The copyright holder for this preprint (which was not certified by peer review) is the author/funder, who has granted bioRxiv a license to display the preprint in perpetuity. It is made available under aCC-BY-NC-ND 4.0 International license.

Supplementary Figure S2

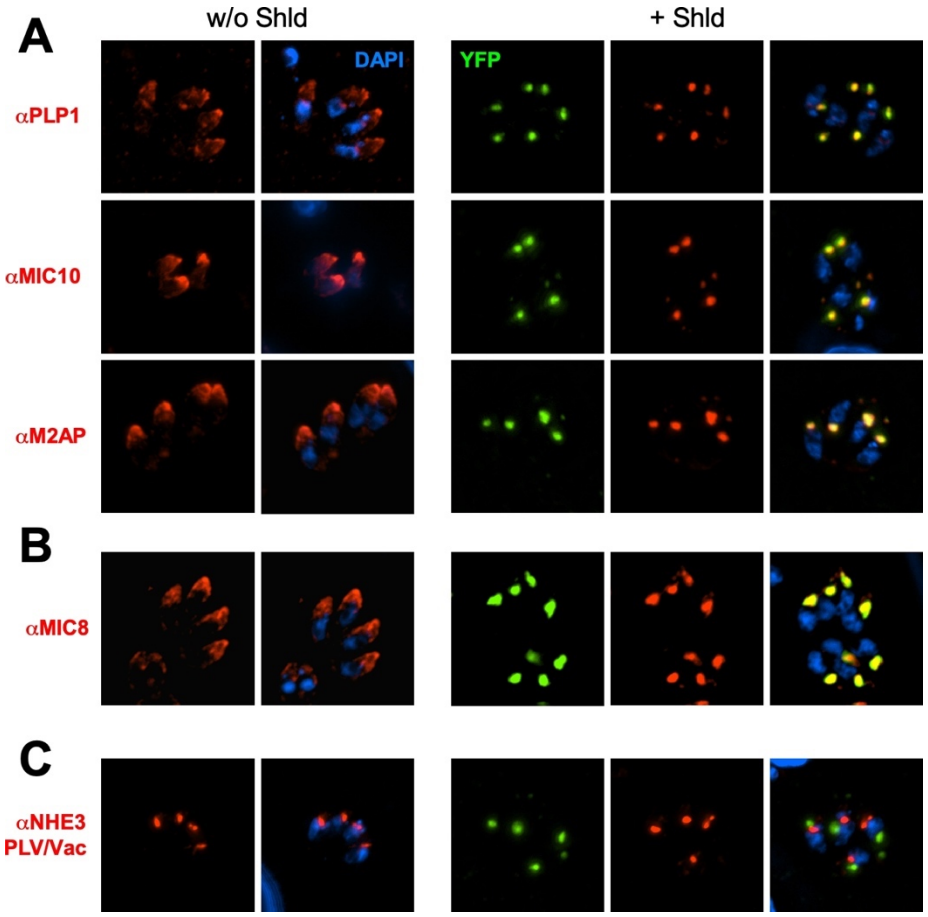

Supplementary Figure S2. Additional localization data in the DD-YFP-FER1 Δ TM dominant negative mutant. **A.** Additional microneme proteins in the MIC2 group. **B.** Additional protein in the MIC3/5/8 group. **C.** NHE3 is a specific marker of the PLV compartment. Parasites were treated with 1 µM Shield-1 for 18 hrs.

bioRxiv preprint doi: https://doi.org/10.1101/2020.04.27.063628; this version posted April 28, 2020. The copyright holder for this preprint (which was not certified by peer review) is the author/funder, who has granted bioRxiv a license to display the preprint in perpetuity. It is made available under aCC-BY-NC-ND 4.0 International license.

Supplementary Figure S3

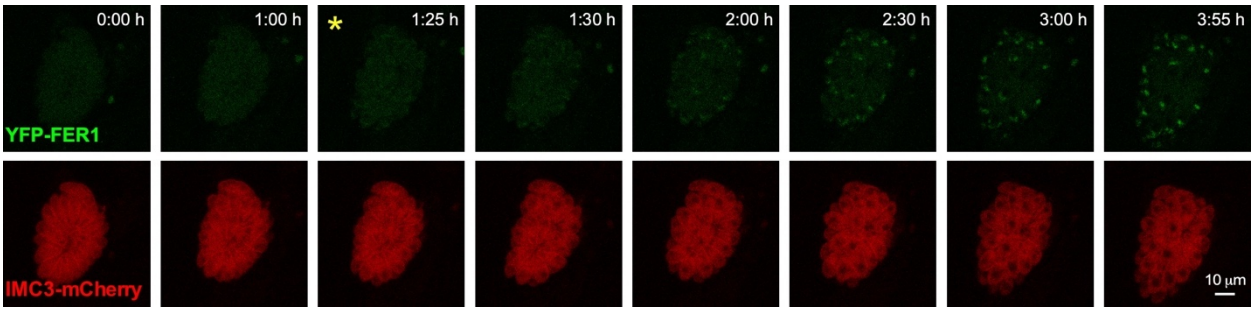

Supplementary Figure S3. Select panels from time lapse experiment of DD-YFP-FER1ΔTM parasites co-transfected with IMC3-mCherry to track cell division. At t=0, 2 µM Shield-1 was added. The first time point at which the piling up of YFP could be convincingly observed is marked with a yellow asterisk. Panels from supplementary movie S2.

bioRxiv preprint doi: https://doi.org/10.1101/2020.04.27.063628; this version posted April 28, 2020. The copyright holder for this preprint (which was not certified by peer review) is the author/funder, who has granted bioRxiv a license to display the preprint in perpetuity. It is made available under aCC-BY-NC-ND 4.0 International license.

Supplementary Table S1. Description of oligonucleotides used. Restriction enzyme sites underlined.

Cloning of tub-YFP-TM(FER1)		
4786	FER1-TM-F(Gib)	GCATGGACGAGCTGTACAAGCCTAGGAGCGCCATTATGAGTGGGCTG
4788	3'dhfr-Not-R(Gib)	CGAATTGGAGCTCCACCGCGGTGGCGGCCGC
Cloning of tub-DD-YFP-FER1^{FL}/sagCAT		
1573	YFP-109420_F	GGTCCCCTAGGATGGCGGCGAAGGCGATC
1574	YFP-109420_R	GGTCCCCCGGGTTATTTGAGGAGAAACATAACAAAGATGACTAGCGC
1635	5xTy_F(avrII)	GGACCCCTAGGGAGGTCCATACTAACCAGGATCCACTTGACGGCGAGG
1636	DD_R(MfeI-EcoRV)	GGACCGATATCTTACAATTGTTCCAGTTTTAGAAGCTCCACACGG
Internal primers used to for FER1 CDS Sanger sequencing		
2717	Fer1-RACE-F	CGCACCAACGAGAGGCGCTCGCAGCTA
2748	FER1_SeqF2	ATGCGTTCCCTGTTTCGAT
2749	FER1_SeqF3	GTACAGCCTCCGCTCTCTTG
2750	FER1_SeqF4	TGTCTGTGTCTCTCCCCAAA
Cloning of tub-DD-YFP-FER1ΔTM/sagCAT		
1651	FLPnoTM(NheI)_F	GGTCCGCTAGCCCTGAAGAGGAAACCTACG
1652	FLPnoTM(XmaI)_R	GGTCCCCCGGGTTACGTCCATTTCAGCCCACTCATAATGGC
Site Directed Mutagenesis of C2D		
4833	SDM-FER1-1-2-F	TCCGGCTCCCTACATCCAAGTGGAACTG
4834	SDM-FER1-1-2-R	AACACGGCGTAGCCGACAGCTGGGAG
6His-FER1 for antiserum generation		
2787	Ava-LIC-Fer1-F	GGGTCCTGGTTCGATGTCGACGAAGGAAGGCAACATTC
2903	Ava-LIC-Fer1-R	CTTGTTCGTGCTGTTTATTAGAGTTGCTCAGGCGTGAAGC
Cloning of pmic3-MIC3-Cherry-DHFR		
4864	gibpMIC3-MIC3-F	GGAGATGACGAGACGTTTAAACGAGGAAAGTGGGGGGGGGGGG
4865	gibpMIC3-MIC3-R	GTTATCCTCCTCGCCCTTGCTCACCCTAGGGAGACTCGCTGGGTACCTTCGTC

bioRxiv preprint doi: https://doi.org/10.1101/2020.04.27.063628; this version posted April 28, 2020. The copyright holder for this preprint (which was not certified by peer review) is the author/funder, who has granted bioRxiv a license to display the preprint in perpetuity. It is made available under aCC-BY-NC-ND 4.0 International license.

Supplementary Table S2. Description of plasmids used.

Plasmid	Source and reference
ptub-DD-YFP-FER1ΔTM/sagCAT	In house [this paper]
ptub-DD-Myc-FER1ΔTM/sagCAT	In house [this paper]
ptub-DD-Myc-FER1ΔTM(^{D541A,D545A})/sagCAT	In house [this paper]
ptub-DD-Myc-FER1^{FL}/sagCAT	In house [this paper]
ptub-DD-Myc-FER1$^{FL\ (D541A,D545A)}$/sagCAT	In house [this paper]
ptub-YFP-TM^{FER1}/sagCAT	In house [this paper]
ptub-IMC3-mCherryRFP/sagCAT	In house [95]
pmic3-MIC3-mCherryRFP/hxgprtDHFR	In house [this paper]
ptub-GRASP55-RFP/sagCAT	Graham Warren [105]
Rab5A-HA OE Transient overexpression	Sabrina Marion [23]
Rab7-HA OE Transient overexpression	Sabrina Marion [23]

bioRxiv preprint doi: https://doi.org/10.1101/2020.04.27.063628; this version posted April 28, 2020. The copyright holder for this preprint (which was not certified by peer review) is the author/funder, who has granted bioRxiv a license to display the preprint in perpetuity. It is made available under aCC-BY-NC-ND 4.0 International license.

1408 **Supplementary Table S3. Description of antibody and antisera used.**

1409

Name (monoclonal)	Species	Dilution (IFA)	Dilution (western)	Source and reference
cMyc (9E10)	mouse	1:50	1:50	Santa Cruz Biotech
HA (3F10)	mouse	1:3000		Roche
MIC2 (6D10)	mouse	1:2000	1:8000	David Sibley [106]
MIC2	rabbit	1:1000	1:8000	David Sibley [106]
MIC3	rabbit	1:100	1:400	Jean-François Dubremetz [107]
MIC5	rabbit	1:500	1:10000	Vern Carruthers [108]
MIC8	rabbit	1:1000		Dominique Soldati [109]
MIC10	rabbit	1:500	1:15000	Vern Carruthers [110]
M2AP	rabbit	1:1000	1:1000	Vern Carruthers [111]
proM2AP	rabbit	1:1000	1:1000	Vern Carruthers [111]
proMIC5	rabbit	1:500		Vern Carruthers [60]
proROP4	rabbit	1:750		Gary Ward [112]
GRA1 (TG17.43)	mouse	1:500	1:15000	BioVision.com [113]
SAG1 (DG52)	mouse	1:500		Jeroen Saeij [114]
GRA3 (T62ch)	mouse	1:500		Maryse Lebrun, Jean-François Dubremetz [115]
SAG1 (T41E5)	mouse & rabbit	1:500		Jean-François Dubremetz [116]
ROP2,3,4	mouse	1:250		Maryse Lebrun [117]
DrpB	rat	1:2000		Peter Bradley [50]
VP1	rabbit	1:4000		Silvia Moreno [51]
APH	rabbit	1:1000		Dominique Soldati [28]
IMC3	rat	1:2000	1:1000	[95]
hCentrin	rabbit	1:1000		Iain Cheeseman, unpublished
Tg-β-tubulin	rabbit	1:500		Naomi Morrissette [118]
α-tubulin (12G10)	mouse	1:2000	1:100	Developmental Studies Hybridoma Bank [119]
NHE3	guinea pig	1:1500		Gustavo Arrizabalaga [54]
FER1	guinea pig	1:1000	1:1000	This paper

1410